Time reversal in viscoelastic media

Habib Ammari, Elie Bretin, Josselin Garnier, Abdul Wahab

Time Reversal Algorithms in Viscoelastic Media*

Habib Ammari† Elie Bretin‡ Josselin Garnier§ Abdul Wahab‡

August 22, 2011

Abstract

In this paper, we consider the problem of reconstructing sources in a homogeneous viscoelastic medium from wavefield measurements using time-reversal algorithms. Our motivation is the recent advances on hybrid methods in biomedical imaging. We first present a modified time-reversal imaging algorithm based on a weighted Helmholtz decomposition and justify mathematically that it provides a better approximation than by simply time reversing the displacement field. Then, we investigate the source inverse problem in an elastic attenuating medium. We provide a regularized time-reversal imaging which corrects the attenuation effect at the first order.

AMS subject classifications. 35L05, 35R30; Secondary 47A52, 65J20

Key words. Elastic wave propagation, Time reversal algorithms, Attenuation correction

1 Introduction

Waves in *loss-less* media are invariant under time transformation $t \to -t$. This simple observation has provided very promising techniques in a variety of domains including biomedical imaging [19], seismology [26], material analysis [30], land-mine detection [28], telecommunication [27] and underwater acoustics [18]. In *time-reversal* algorithms, an *output* wave is *time reversed* and *retransmitted* into the medium. By *time invariance* and *reciprocity* properties, the retransmitted wave retraces its path back through the medium and converges to the location of *initial sources*. This convergence of the reverted wave holds whatever the complexity of the underlying medium, which can be homogeneous or scattering, dispersive or non-dispersive. See for instance [2, 17, 18, 19, 20, 33] and references therein for comprehensive details and discussions on time reversal. See also [4, 10, 16, 38] for applications of time-reversal techniques in biomedical imaging.

The robustness and simplicity of time-reversal techniques make them an ideal choice to resolve *source localization problems*. These inverse problems have been of significant interest in recent years and find numerous applications in different fields, particularly in biomedical imaging [3, 6, 7, 8, 29, 34]. If the sources are *temporally localized*, the source localization

*This work was supported by the ERC Advanced Grant Project MULTIMOD–267184.

†Department of Mathematics and Applications, Ecole Normale Supérieure, 45 Rue d'Ulm, 75005 Paris, France (habib.ammari@ens.fr).

‡Centre de Mathématiques Appliquées, CNRS UMR 7641, École Polytechnique, 91128 Palaiseau, France (bretin@cmap.polytechnique.fr, wahab@cmap.polytechnique.fr)

§Laboratoire de Probabilités et Modèles Aléatoires & Laboratoire Jacques-Louis Lions, Université Paris VII, 75205 Paris Cedex 13, France (garnier@math.jussieu.fr)

problems are actually equivalent to find *initial states* of a *system* governed by differential equations from the *observations* over some finite interval of time.

In this work, we consider the problem of reconstructing sources in a viscoelastic medium from wavefield measurements using time-reversal methods. Our motivation is the recent advances on hybrid methods in biomedical imaging exploiting elastic properties of the soft tissues [21]. Examples of these hybrid methods include magnetic resonance elastography [9, 16], transient elasticity imaging [10], shear wave imaging [31] and acoustic radiation force imaging [8, 12]. The envisaged problem is quite challenging, indeed, because time reversibility of the wave equation breaks down in lossy media. Further, if not accounted for, these losses produce serious blurring in source reconstruction using classical time-reversal methods. In this paper, we use a thermo-viscous law model for the attenuation losses. We refer, for instance, to [24, 25, 14] for detailed discussions on the attenuation models in wave propagation and their causality properties.

The main contributions of this paper are twofold. We first provide a modified time-reversal imaging algorithm in non-attenuating media based on a weighted Helmholtz decomposition and justify both analytically and numerically that it provides a better approximation than by simply time reversing the displacement field. Then, we give a regularized time-reversal imaging algorithm for source reconstruction in attenuated media and show that it leads to a first-order approximation in terms of the viscosity parameters of the source term. We present a variety of numerical illustrations to compare different time-reversal algorithms and to highlight the potential of our original approach.

2 Time reversal in homogeneous elastic media without viscosity

Let us consider the homogeneous isotropic elastic wave equation in a d-dimensional open medium:

$$\begin{cases} \dfrac{\partial^2 \mathbf{u}}{\partial t^2}(\boldsymbol{x},t) - \mathcal{L}_{\lambda,\mu}\mathbf{u}(\boldsymbol{x},t) = \dfrac{d\delta_0(t)}{dt}\mathbf{F}(\boldsymbol{x}), & (\boldsymbol{x},t) \in \mathbb{R}^d \times \mathbb{R}, \\ \mathbf{u}(\boldsymbol{x},t) = \dfrac{\partial \mathbf{u}}{\partial t}(\boldsymbol{x},t) = \mathbf{0}, & \boldsymbol{x} \in \mathbb{R}^d,\ t < 0, \end{cases} \tag{2.1}$$

where

$$\mathcal{L}_{\lambda,\mu}\mathbf{u} = \mu\Delta\mathbf{u} + (\lambda+\mu)\nabla(\nabla\cdot\mathbf{u}). \tag{2.2}$$

Here (λ,μ) are the Lamé coefficients of the medium and the density of the medium is equal to one. The aim in this work is to design efficient algorithms for reconstructing the compactly supported source function $\mathbf{F}$ from the recorded data

$$\Big\{\mathbf{g}(\boldsymbol{y},t) = \mathbf{u}(\boldsymbol{y},t), t \in [0,T], \boldsymbol{y} \in \partial\Omega\Big\}, \tag{2.3}$$

where Ω is supposed to strictly contain the support of $\mathbf{F}$. We are interested in the following time-reversal functional:

$$\mathcal{I}(\boldsymbol{x}) = \int_0^T \mathbf{v}_s(\boldsymbol{x},T)ds, \quad \boldsymbol{x} \in \Omega, \tag{2.4}$$

where the vector field $\mathbf{v}_s$ is defined as the solution of

$$\begin{cases} \dfrac{\partial^2 \mathbf{v}_s}{\partial t^2}(\boldsymbol{x},t) - \mathcal{L}_{\lambda,\mu}\mathbf{v}_s(\boldsymbol{x},t) = \dfrac{d\delta_s(t)}{dt}\mathbf{g}(\boldsymbol{x},T-s)\delta_{\partial\Omega}(\boldsymbol{x}), & (\boldsymbol{x},t)\in\mathbb{R}^d\times\mathbb{R}, \\ \mathbf{v}_s(\boldsymbol{x},t) = \dfrac{\partial \mathbf{v}_s}{\partial t}(\boldsymbol{x},t) = \mathbf{0}, & \boldsymbol{x}\in\mathbb{R}^d,\ t<s. \end{cases} \tag{2.5}$$

Here, $\delta_{\partial\Omega}$ is the surface Dirac mass on $\partial\Omega$ and $\mathbf{g}=\mathbf{u}$ on $\partial\Omega\times\mathbb{R}$ is the measured displacement field.

The time-reversal imaging functional $\mathcal{I}$ is usually implemented to reconstruct the source distribution in an elastic medium [16, 28, 29]. It is motivated by the time reversibility property of the elastic waves. In a general setting, however, it is not sure that it provides a good reconstruction of the source distribution $\mathbf{F}$. Indeed the problem is that the recorded displacement field at the surface of the domain is a mixture of pressure and shear wave components. By time reversing and backpropagating these signals as in (2.4) a blurred image is obtained due to the fact that the pressure and shear wave speeds are different.

In this work, we first present a modified time-reversal imaging functional $\widetilde{\mathcal{I}}$, and justify mathematically that it provides a better approximation than $\mathcal{I}$ of the source $\mathbf{F}$. This new functional $\widetilde{\mathcal{I}}$ can be seen as a correction based on a *weighted Helmholtz decomposition* to $\mathcal{I}$ (which is considered as an *initial guess*). In fact, we find the compressional and the shear components of $\mathcal{I}$ such that

$$\mathcal{I} = \nabla\times\psi_{\mathcal{I}} + \nabla\phi_{\mathcal{I}}. \tag{2.6}$$

Then we multiply these components with $c_p=\sqrt{\lambda+2\mu}$ and $c_s=\sqrt{\mu}$, the pressure and the shear wave speeds respectively. Finally, we define $\widetilde{\mathcal{I}}$ by

$$\widetilde{\mathcal{I}} = c_s\nabla\times\psi_{\mathcal{I}} + c_p\nabla\phi_{\mathcal{I}}. \tag{2.7}$$

We rigorously explain why should this new functional be better than the original one. We substantiate this argument with numerical illustrations.

In the sequel, we define respectively the Helmholtz decomposition operators $\mathcal{H}^p$ and $\mathcal{H}^s$ by

$$\mathcal{H}^p[\mathcal{I}] := \nabla\phi_{\mathcal{I}} \quad \text{and} \quad \mathcal{H}^s[\mathcal{I}] := \nabla\times\psi_{\mathcal{I}}. \tag{2.8}$$

2.1 Time-reversal imaging analysis

In order to establish some results about time reversal using $\mathcal{I}$ and $\widetilde{\mathcal{I}}$, we use the following integral formulation based on the elastic Green's tensor.

2.1.1 Integral formulation

Let us introduce the outgoing Green's tensor $\mathbb{G}_{\omega,0}$ associated to the elastic wave equation with a point source at $\mathbf{0}$:

$$(\mathcal{L}_{\lambda,\mu}+\omega^2)\mathbb{G}_{\omega,0}(\boldsymbol{x}) = -\delta_{\mathbf{0}}\mathbb{I}, \qquad \boldsymbol{x}\in\mathbb{R}^d. \tag{2.9}$$

It can be expressed in the form [1, 11]

$$\mathbb{G}_{\omega,0}(\boldsymbol{x}) = \frac{1}{\mu\kappa_s^2}\left(\kappa_s^2 G^s_{\omega,0}(\boldsymbol{x})\mathbb{I} + \mathbb{D}\left(G^s_{\omega,0}-G^p_{\omega,0}\right)(\boldsymbol{x})\right), \qquad \boldsymbol{x}\in\mathbb{R}^d, \tag{2.10}$$

where $\mathbb{I} = (\delta_{ij})_{i,j=1}^d$, $\mathbb{D} = (\frac{\partial^2}{\partial x_i \partial x_j})_{i,j=1}^d$, and $\kappa_s^2 = \frac{\omega^2}{\mu}$ and $\kappa_p^2 = \frac{\omega^2}{\lambda+2\mu}$ are the shear and the pressure wavenumbers respectively. Here, $G_{\omega,0}^{\alpha}(\boldsymbol{x})$ is the fundamental solution of the Helmholtz operator $\Delta + \kappa_\alpha^2$ in $\mathbb{R}^d$ with $\alpha = p, s$. For example when $d = 3$, we have

$$G_{\omega,0}^{\alpha}(\boldsymbol{x}) = \frac{\exp(i\kappa_\alpha|\boldsymbol{x}|)}{4\pi|\boldsymbol{x}|}, \quad \alpha = p, s. \tag{2.11}$$

The functional $\mathcal{I}(\boldsymbol{x})$ defined by (2.4) can be expressed in the form [4]

$$\begin{aligned}\mathcal{I}(\boldsymbol{x}) &= \Re e\left[\frac{1}{2\pi}\int_{\mathbb{R}^d}\int_{\mathbb{R}}\omega^2\left[\int_{\partial\Omega}\mathbb{G}_\omega(\boldsymbol{x},\boldsymbol{y})\overline{\mathbb{G}}_\omega(\boldsymbol{y},\boldsymbol{z})d\sigma(\boldsymbol{y})\right]d\omega\mathbf{F}(\boldsymbol{z})\,d\boldsymbol{z}\right]\\ &= \frac{1}{4\pi}\int_{\mathbb{R}^d}\int_{\mathbb{R}}\omega^2\left[\int_{\partial\Omega}\left[\mathbb{G}_\omega(\boldsymbol{x},\boldsymbol{y})\overline{\mathbb{G}}_\omega(\boldsymbol{y},\boldsymbol{z}) + \overline{\mathbb{G}}_\omega(\boldsymbol{x},\boldsymbol{y})\mathbb{G}_\omega(\boldsymbol{y},\boldsymbol{z})\right]d\sigma(\boldsymbol{y})\right]d\omega\mathbf{F}(\boldsymbol{z})\,d\boldsymbol{z},\end{aligned} \tag{2.12}$$

where we have introduced the outgoing Green's tensor for a point source at $\boldsymbol{y}$:

$$\mathbb{G}_\omega(\boldsymbol{x},\boldsymbol{y}) = \mathbb{G}_{\omega,0}(\boldsymbol{x}-\boldsymbol{y}). \tag{2.13}$$

We also introduce the decomposition of $\mathbb{G}_{\omega,0}$ into shear and compressional components as

$$\mathbb{G}_{\omega,0}(\boldsymbol{x}) = \mathbb{G}_{\omega,0}^p(\boldsymbol{x}) + \mathbb{G}_{\omega,0}^s(\boldsymbol{x}), \tag{2.14}$$

with

$$\mathbb{G}_{\omega,0}^p = -\frac{1}{\omega^2}\mathbb{D}G_{\omega,0}^p \quad \text{and} \quad \mathbb{G}_{\omega,0}^s = \frac{1}{\omega^2}\left(\kappa_s^2\mathbb{I} + \mathbb{D}\right)G_{\omega,0}^s. \tag{2.15}$$

We can extend Helmholtz operator $\mathcal{H}^p$ and $\mathcal{H}^s$ to tensors $\mathbb{G}$ as follows:

$$\mathcal{H}^p[\mathbb{G}]\boldsymbol{p} = \mathcal{H}^p[\mathbb{G}\boldsymbol{p}] \quad \text{and} \quad \mathcal{H}^s[\mathbb{G}]\boldsymbol{p} = \mathcal{H}^s[\mathbb{G}\boldsymbol{p}] \quad \text{for all vectors } \boldsymbol{p}.$$

Note that $\mathbb{G}_{\omega,0}^p$ and $\mathbb{G}_{\omega,0}^s$ satisfy, respectively

$$(\mathcal{L}_{\lambda,\mu} + \omega^2)\mathbb{G}_{\omega,0}^p = \mathcal{H}^p\left[-\delta_{\mathbf{0}}\mathbb{I}\right] \quad \text{and} \quad (\mathcal{L}_{\lambda,\mu} + \omega^2)\mathbb{G}_{\omega,0}^s = \mathcal{H}^s\left[-\delta_{\mathbf{0}}\mathbb{I}\right]. \tag{2.16}$$

Consequently, the Helmholtz decomposition of $\mathcal{I}$ can be derived explicitly

$$\mathcal{I}(\boldsymbol{x}) = \mathcal{H}^p[\mathcal{I}](\boldsymbol{x}) + \mathcal{H}^s[\mathcal{I}](\boldsymbol{x}), \tag{2.17}$$

with

$$\mathcal{H}^p[\mathcal{I}](\boldsymbol{x}) = \frac{1}{4\pi}\int_{\mathbb{R}^d}\int_{\mathbb{R}}\omega^2\left[\int_{\partial\Omega}\left[\mathbb{G}_\omega^p(\boldsymbol{x},\boldsymbol{y})\overline{\mathbb{G}}_\omega(\boldsymbol{y},\boldsymbol{z}) + \overline{\mathbb{G}}_\omega^p(\boldsymbol{x},\boldsymbol{y})\mathbb{G}_\omega(\boldsymbol{y},\boldsymbol{z})\right]d\sigma(\boldsymbol{y})\right]d\omega\mathbf{F}(\boldsymbol{z})\,d\boldsymbol{z},$$

and

$$\mathcal{H}^s[\mathcal{I}](\boldsymbol{x}) = \frac{1}{4\pi}\int_{\mathbb{R}^d}\int_{\mathbb{R}}\omega^2\left[\int_{\partial\Omega}\left[\mathbb{G}_\omega^s(\boldsymbol{x},\boldsymbol{y})\overline{\mathbb{G}}_\omega(\boldsymbol{y},\boldsymbol{z}) + \overline{\mathbb{G}}_\omega^s(\boldsymbol{x},\boldsymbol{y})\mathbb{G}_\omega(\boldsymbol{y},\boldsymbol{z})\right]d\sigma(\boldsymbol{y})\right]d\omega\mathbf{F}(\boldsymbol{z})\,d\boldsymbol{z}.$$

Finally, the integral formulation of the modified imaging functional $\widetilde{\mathcal{I}}$ defined by (2.7) reads

$$\widetilde{\mathcal{I}}(\boldsymbol{x}) = \Re e\left[\frac{1}{2\pi}\int_{\mathbb{R}^d}\int_{\mathbb{R}}\omega^2\left[\int_{\partial\Omega}\left[c_s\mathbb{G}_\omega^s(\boldsymbol{x},\boldsymbol{y}) + c_p\mathbb{G}_\omega^p(\boldsymbol{x},\boldsymbol{y})\right]\overline{\mathbb{G}}_\omega(\boldsymbol{y},\boldsymbol{z})d\sigma(\boldsymbol{y})\right]d\omega\mathbf{F}(\boldsymbol{z})\,d\boldsymbol{z}\right]. \tag{2.18}$$

2.1.2 Helmholtz-Kirchhoff identity

In order to approximate the integral formulation (2.18) we use a Helmholtz-Kirchhoff identity for elastic media. Some of the results presented in this subsection can be found in [35, 36] in the context of elastodynamic seismic interferometry. Indeed, the elastodynamic reciprocity theorems (Propositions 2.1 and 2.5) are the key ingredient to understand the relation between the cross correlations of signals emitted by uncorrelated noise sources and the Green's function between the observation points.

Let us introduce the conormal derivative $\frac{\partial \mathbf{u}}{\partial \nu}(\boldsymbol{y})$, $\boldsymbol{y} \in \partial\Omega$, of the displacement field $\mathbf{u}$ at the surface $\partial\Omega$ in the outward unit normal direction $\boldsymbol{n}$ by

$$\frac{\partial \mathbf{u}}{\partial \nu} := \lambda(\nabla \cdot \mathbf{u})\boldsymbol{n} + \mu\big(\nabla \mathbf{u}^T + (\nabla \mathbf{u}^T)^T\big)\boldsymbol{n}, \tag{2.19}$$

where T denotes the transpose.

Note also that the conormal derivative tensor $\frac{\partial \mathbb{G}}{\partial \nu}$ means that for all constant vectors $\boldsymbol{p}$,

$$\left[\frac{\partial \mathbb{G}_\omega}{\partial \nu}\right]\boldsymbol{p} := \frac{\partial\left[\mathbb{G}_\omega \boldsymbol{p}\right]}{\partial \nu}.$$

The following proposition is equivalent to [36, Eq. (73)]. Since our formulation is slightly different and this is the first building block of our theory we give its proof for consistency. Moreover, elements of the proof are used in Proposition 2.2.

Proposition 2.1. *For all $\boldsymbol{x}, \boldsymbol{z} \in \Omega$, we have*

$$\int_{\partial\Omega}\left[\frac{\partial \mathbb{G}_\omega(\boldsymbol{x},\boldsymbol{y})}{\partial \nu}\overline{\mathbb{G}}_\omega(\boldsymbol{y},\boldsymbol{z}) - \mathbb{G}_\omega(\boldsymbol{x},\boldsymbol{y})\frac{\partial \overline{\mathbb{G}}_\omega(\boldsymbol{y},\boldsymbol{z})}{\partial \nu}\right] d\sigma(\boldsymbol{y}) = 2i\Im m\{\mathbb{G}_\omega(\boldsymbol{x},\boldsymbol{z})\}. \tag{2.20}$$

Proof. By reciprocity we have

$$\mathbb{G}_\omega(\boldsymbol{y},\boldsymbol{x}) = \left[\mathbb{G}_\omega(\boldsymbol{x},\boldsymbol{y})\right]^T. \tag{2.21}$$

Additionally, in the homogeneous case we have $\mathbb{G}_\omega(\boldsymbol{y},\boldsymbol{x}) = \mathbb{G}_\omega(\boldsymbol{x},\boldsymbol{y})$, but we will not use this property here. Our goal is to show that for all constant vectors $\boldsymbol{p}$ and $\boldsymbol{q}$, we have

$$\int_{\partial\Omega}\left[\boldsymbol{q}\cdot\frac{\partial \mathbb{G}_\omega(\boldsymbol{x},\boldsymbol{y})}{\partial \nu}\overline{\mathbb{G}}_\omega(\boldsymbol{y},\boldsymbol{z})\boldsymbol{p} - \boldsymbol{q}\cdot\mathbb{G}_\omega(\boldsymbol{x},\boldsymbol{y})\frac{\partial \overline{\mathbb{G}}_\omega(\boldsymbol{y},\boldsymbol{z})}{\partial \nu}\boldsymbol{p}\right] d\sigma(\boldsymbol{y}) = 2i\boldsymbol{q}\cdot\Im m\{\mathbb{G}_\omega(\boldsymbol{x},\boldsymbol{z})\}\boldsymbol{p}.$$

Taking scalar product of equations

$$(\mathcal{L}_{\lambda,\mu}+\omega^2)\mathbb{G}_\omega(\boldsymbol{y},\boldsymbol{x})\boldsymbol{q} = -\delta_{\boldsymbol{x}}\boldsymbol{q} \quad \text{and} \quad (\mathcal{L}_{\lambda,\mu}+\omega^2)\overline{\mathbb{G}}_\omega(\boldsymbol{y},\boldsymbol{z})\boldsymbol{p} = -\delta_{\boldsymbol{z}}\boldsymbol{p}$$

with $\overline{\mathbb{G}}_\omega(\boldsymbol{y},\boldsymbol{z})\boldsymbol{p}$ and $\mathbb{G}_\omega(\boldsymbol{y},\boldsymbol{x})\boldsymbol{q}$ respectively, subtracting the second result from the first, and integrating in $\boldsymbol{y}$ over Ω, we obtain

$$\begin{aligned}&\int_\Omega\left[(\overline{\mathbb{G}}_\omega(\boldsymbol{y},\boldsymbol{z})\boldsymbol{p})\cdot\mathcal{L}_{\lambda,\mu}(\mathbb{G}_\omega(\boldsymbol{y},\boldsymbol{x})\boldsymbol{q}) - \mathcal{L}_{\lambda,\mu}(\overline{\mathbb{G}}_\omega(\boldsymbol{y},\boldsymbol{z})\boldsymbol{p})\cdot(\mathbb{G}_\omega(\boldsymbol{y},\boldsymbol{x})\boldsymbol{q})\right]\, d\boldsymbol{y}\\ &= \boldsymbol{p}\cdot(\mathbb{G}_\omega(\boldsymbol{z},\boldsymbol{x})\boldsymbol{q}) - \boldsymbol{q}\cdot(\overline{\mathbb{G}}_\omega(\boldsymbol{x},\boldsymbol{z})\boldsymbol{p}) = 2i\boldsymbol{q}\cdot\Im m\{\mathbb{G}_\omega(\boldsymbol{x},\boldsymbol{z})\}\boldsymbol{p}.\end{aligned}$$

Using the form of the operator $\mathcal{L}_{\lambda,\mu}$, this gives

$$
\begin{aligned}
&2i\boldsymbol{q}\cdot\Im m\{\mathbb{G}_\omega(\boldsymbol{x},\boldsymbol{z})\}\boldsymbol{p}\\
&=\lambda\int_\Omega\left[(\overline{\mathbb{G}}_\omega(\boldsymbol{y},\boldsymbol{z})\boldsymbol{p})\cdot\{\nabla\nabla\cdot(\mathbb{G}_\omega(\boldsymbol{y},\boldsymbol{x})\boldsymbol{q})\}-(\mathbb{G}_\omega(\boldsymbol{y},\boldsymbol{x})\boldsymbol{q})\cdot\left\{\nabla\nabla\cdot(\overline{\mathbb{G}}_\omega(\boldsymbol{y},\boldsymbol{z})\boldsymbol{p})\right\}\right]d\boldsymbol{y}\\
&\quad+\mu\int_\Omega\left[(\overline{\mathbb{G}}_\omega(\boldsymbol{y},\boldsymbol{z})\boldsymbol{p})\cdot\{(\Delta+\nabla\nabla\cdot)(\mathbb{G}_\omega(\boldsymbol{y},\boldsymbol{x})\boldsymbol{q})\}-(\mathbb{G}_\omega(\boldsymbol{y},\boldsymbol{x})\boldsymbol{q})\cdot\left\{(\Delta+\nabla\nabla\cdot)(\overline{\mathbb{G}}_\omega(\boldsymbol{y},\boldsymbol{z})\boldsymbol{p})\right\}\right]d\boldsymbol{y}.
\end{aligned}
$$

We recall that, for two functions $\mathbf{u},\mathbf{v}:\mathbb{R}^d\to\mathbb{R}^d$, we have

$$
\begin{aligned}
(\Delta\mathbf{u}+\nabla(\nabla\cdot\mathbf{u}))\cdot\mathbf{v} &= \nabla\cdot\left[(\nabla\mathbf{u}^T+(\nabla\mathbf{u}^T)^T)\mathbf{v}\right]-\frac{1}{2}(\nabla\mathbf{u}^T+(\nabla\mathbf{u}^T)^T)\cdot(\nabla\mathbf{v}^T+(\nabla\mathbf{v}^T)^T),\\
\nabla(\nabla\cdot\mathbf{u})\cdot\mathbf{v} &= \nabla\cdot\left[(\nabla\cdot\mathbf{u})\mathbf{v}\right]-(\nabla\cdot\mathbf{u})(\nabla\cdot\mathbf{v}).
\end{aligned}
$$

Therefore, we find

$$
\begin{aligned}
&2i\boldsymbol{q}\cdot\Im m\{\mathbb{G}_\omega(\boldsymbol{x},\boldsymbol{z})\}\boldsymbol{p}\\
&=\lambda\int_\Omega\left[\nabla\cdot\left\{[\nabla\cdot(\mathbb{G}_\omega(\boldsymbol{y},\boldsymbol{x})\boldsymbol{q})](\overline{\mathbb{G}}_\omega(\boldsymbol{y},\boldsymbol{z})\boldsymbol{p})\right\}-\nabla\cdot\left\{[\nabla\cdot(\overline{\mathbb{G}}_\omega(\boldsymbol{y},\boldsymbol{z})\boldsymbol{p})](\mathbb{G}_\omega(\boldsymbol{y},\boldsymbol{x})\boldsymbol{q})\right\}\right]d\boldsymbol{y}\\
&\quad+\mu\int_\Omega\left[\nabla\cdot\left\{\left(\nabla(\mathbb{G}_\omega(\boldsymbol{y},\boldsymbol{x})\boldsymbol{q})^T+(\nabla(\mathbb{G}_\omega(\boldsymbol{y},\boldsymbol{x})\boldsymbol{q})^T)^T\right)\overline{\mathbb{G}}_\omega(\boldsymbol{y},\boldsymbol{z})\boldsymbol{p}\right\}\right.\\
&\qquad\left.-\nabla\cdot\left\{\left(\nabla(\overline{\mathbb{G}}_\omega(\boldsymbol{y},\boldsymbol{z})\boldsymbol{p})^T+(\nabla(\overline{\mathbb{G}}_\omega(\boldsymbol{y},\boldsymbol{z})\boldsymbol{p})^T)^T\right)\mathbb{G}_\omega(\boldsymbol{y},\boldsymbol{x})\boldsymbol{q}\right\}\right]d\boldsymbol{y}.
\end{aligned}
$$

Now, we use divergence theorem and the definition of the conormal derivative to get

$$
\begin{aligned}
&2i\boldsymbol{q}\cdot\Im m\{\mathbb{G}_\omega(\boldsymbol{x},\boldsymbol{z})\}\boldsymbol{p}\\
&=\lambda\int_{\partial\Omega}\left[\boldsymbol{n}\cdot\left\{[\nabla\cdot(\mathbb{G}_\omega(\boldsymbol{y},\boldsymbol{x})\boldsymbol{q})](\overline{\mathbb{G}}_\omega(\boldsymbol{y},\boldsymbol{z})\boldsymbol{p})\right\}-\boldsymbol{n}\cdot\left\{[\nabla\cdot(\overline{\mathbb{G}}_\omega(\boldsymbol{y},\boldsymbol{z})\boldsymbol{p})](\mathbb{G}_\omega(\boldsymbol{y},\boldsymbol{x})\boldsymbol{q})\right\}\right]d\sigma(\boldsymbol{y})\\
&\quad+\mu\int_\Omega\left[\boldsymbol{n}\cdot\left\{\left(\nabla(\mathbb{G}_\omega(\boldsymbol{y},\boldsymbol{x})\boldsymbol{q})^T+(\nabla(\mathbb{G}_\omega(\boldsymbol{y},\boldsymbol{x})\boldsymbol{q})^T)^T\right)\overline{\mathbb{G}}_\omega(\boldsymbol{y},\boldsymbol{z})\boldsymbol{p}\right\}\right.\\
&\qquad\left.-\boldsymbol{n}\cdot\left\{\left(\nabla(\overline{\mathbb{G}}_\omega(\boldsymbol{y},\boldsymbol{z})\boldsymbol{p})^T+(\nabla(\overline{\mathbb{G}}_\omega(\boldsymbol{y},\boldsymbol{z})\boldsymbol{p})^T)^T\right)\mathbb{G}_\omega(\boldsymbol{y},\boldsymbol{x})\boldsymbol{q}\right\}\right]d\sigma(\boldsymbol{y})\\
&=\lambda\int_{\partial\Omega}\left[(\overline{\mathbb{G}}_\omega(\boldsymbol{y},\boldsymbol{z})\boldsymbol{p})\cdot\{\nabla\cdot(\mathbb{G}_\omega(\boldsymbol{y},\boldsymbol{x})\boldsymbol{q})\boldsymbol{n}\}-(\mathbb{G}_\omega(\boldsymbol{y},\boldsymbol{x})\boldsymbol{q})\cdot\left\{\nabla\cdot(\overline{\mathbb{G}}_\omega(\boldsymbol{y},\boldsymbol{z})\boldsymbol{p})\boldsymbol{n}\right\}\right]d\sigma(\boldsymbol{y})\\
&\quad+\mu\int_{\partial\Omega}\left[(\overline{\mathbb{G}}_\omega(\boldsymbol{y},\boldsymbol{z})\boldsymbol{p})\cdot\left\{\left(\nabla(\mathbb{G}_\omega(\boldsymbol{y},\boldsymbol{x})\boldsymbol{q})^T+(\nabla(\mathbb{G}_\omega(\boldsymbol{y},\boldsymbol{x})\boldsymbol{q})^T)^T\right)\boldsymbol{n}\right\}\right.\\
&\qquad\left.-(\mathbb{G}_\omega(\boldsymbol{y},\boldsymbol{x})\boldsymbol{q})\cdot\left\{\left(\nabla(\overline{\mathbb{G}}_\omega(\boldsymbol{y},\boldsymbol{z})\boldsymbol{p})^T+(\nabla(\overline{\mathbb{G}}_\omega(\boldsymbol{y},\boldsymbol{z})\boldsymbol{p})^T)^T\right)\boldsymbol{n}\right\}\right]d\sigma(\boldsymbol{y})\\
&=\int_{\partial\Omega}\left[(\overline{\mathbb{G}}_\omega(\boldsymbol{y},\boldsymbol{z})\boldsymbol{p})\cdot\frac{\partial\mathbb{G}_\omega(\boldsymbol{y},\boldsymbol{x})\boldsymbol{q}}{\partial\nu}-(\mathbb{G}_\omega(\boldsymbol{y},\boldsymbol{x})\boldsymbol{q})\cdot\frac{\partial\overline{\mathbb{G}}_\omega(\boldsymbol{y},\boldsymbol{z})\boldsymbol{p}}{\partial\nu}\right]d\sigma(\boldsymbol{y})\\
&=\int_{\partial\Omega}\left[\boldsymbol{q}\cdot\frac{\partial\mathbb{G}_\omega(\boldsymbol{x},\boldsymbol{y})}{\partial\nu}\overline{\mathbb{G}}_\omega(\boldsymbol{y},\boldsymbol{z})\boldsymbol{p}-\boldsymbol{q}\cdot\mathbb{G}_\omega(\boldsymbol{x},\boldsymbol{y})\frac{\partial\overline{\mathbb{G}}_\omega(\boldsymbol{y},\boldsymbol{z})}{\partial\nu}\boldsymbol{p}\right]d\sigma(\boldsymbol{y}),
\end{aligned}
$$

which is the desired result. Note that for establishing the last equality we have used the reciprocity relation (2.21). □

The proof of Proposition 2.1 uses only the reciprocity relation and the divergence theorem. Consequently, Proposition 2.1 also holds in a heterogeneous medium, as shown in [36].

The following proposition cannot be found in the literature, probably because its application in the context of seismic interferometry has not been identified. It is an important ingredient in the analysis of our improved imaging functional. Note that the proofs of Propositions 2.2 and 2.3 require the medium to be homogeneous (so that $\mathcal{H}^s$ and $\mathcal{H}^p$ commute with $\mathcal{L}_{\lambda,\mu}$), and we cannot expect these propositions to be true in a heterogeneous medium because of mode conversion between pressure and shear waves.

Proposition 2.2. *For all $\boldsymbol{x}, \boldsymbol{z} \in \Omega$, we have*

$$\int_{\partial\Omega} \left[\frac{\partial \mathbb{G}^s_\omega(\boldsymbol{x},\boldsymbol{y})}{\partial \nu} \overline{\mathbb{G}^p_\omega}(\boldsymbol{y},\boldsymbol{z}) - \mathbb{G}^s_\omega(\boldsymbol{x},\boldsymbol{y}) \frac{\partial \overline{\mathbb{G}^p_\omega}(\boldsymbol{y},\boldsymbol{z})}{\partial \nu} \right] d\sigma(\boldsymbol{y}) = 0. \tag{2.22}$$

Proof. First, we recall that $\mathbb{G}^p_\omega(\boldsymbol{y},\boldsymbol{x})$ and $\mathbb{G}^s_\omega(\boldsymbol{y},\boldsymbol{x})$ are solutions of (2.16). We proceed as in the proof of the previous proposition to find:

$$\begin{aligned}
&\int_{\partial\Omega} \left[\frac{\partial \mathbb{G}^s_\omega(\boldsymbol{x},\boldsymbol{y})}{\partial \nu} \overline{\mathbb{G}^p_\omega}(\boldsymbol{y},\boldsymbol{z}) - \mathbb{G}^s_\omega(\boldsymbol{x},\boldsymbol{y}) \frac{\partial \overline{\mathbb{G}^p_\omega}(\boldsymbol{y},\boldsymbol{z})}{\partial \nu} \right] d\sigma(\boldsymbol{y}) \\
&\qquad = \int_\Omega \left[\mathcal{H}^s[-\delta_{\boldsymbol{x}}\mathbb{I}](\boldsymbol{y}) \overline{\mathbb{G}^p_\omega}(\boldsymbol{y},\boldsymbol{z}) - \mathbb{G}^s_\omega(\boldsymbol{x},\boldsymbol{y}) \mathcal{H}^p[-\delta_{\boldsymbol{z}}\mathbb{I}](\boldsymbol{y}) \right] d\boldsymbol{y} \\
&\qquad = [\mathcal{H}^s[-\delta_{\mathbf{0}}\mathbb{I}] * \overline{\mathbb{G}^p_\omega}(\cdot,\boldsymbol{z})](\boldsymbol{x}) - [\mathbb{G}^s_\omega(\boldsymbol{x},\cdot) * \mathcal{H}^p[-\delta_{\mathbf{0}}\mathbb{I}]](\boldsymbol{z}).
\end{aligned}$$

Using the fact that $\mathbb{G}^p_\omega = \mathcal{H}^p[\mathbb{G}_\omega]$ and $\mathcal{H}^s\mathcal{H}^p = \mathcal{H}^p\mathcal{H}^s = 0$ we get

$$\mathcal{H}^s[\mathcal{H}^s[-\delta_{\mathbf{0}}\mathbb{I}] * \overline{\mathbb{G}^p_\omega}(\cdot,\boldsymbol{z})] = 0 \quad \text{and } \mathcal{H}^p[\mathcal{H}^s[-\delta_{\mathbf{0}}\mathbb{I}] * \overline{\mathbb{G}^p_\omega}(\cdot,\boldsymbol{z})] = 0.$$

Therefore, we conclude

$$[\mathcal{H}^s[-\delta_{\mathbf{0}}\mathbb{I}] * \overline{\mathbb{G}^p_\omega}(\cdot,\boldsymbol{z})](\boldsymbol{x}) = 0.$$

Similarly, we have

$$[\mathbb{G}^s_\omega(\boldsymbol{x},\cdot) * \mathcal{H}^p[-\delta_{\mathbf{0}}\mathbb{I}]](\boldsymbol{z}) = 0,$$

which gives the desired result. □

Finally the following proposition shows that the elastodynamic reciprocity theorem (Proposition 2.1) holds for each wave component in a homogeneous medium.

Proposition 2.3. *For all $\boldsymbol{x}, \boldsymbol{z} \in \mathbb{R}^d$ and $\alpha = p, s$,*

$$\int_{\partial\Omega} \left[\frac{\partial \mathbb{G}^\alpha_\omega(\boldsymbol{x},\boldsymbol{y})}{\partial \nu} \overline{\mathbb{G}^\alpha_\omega}(\boldsymbol{y},\boldsymbol{z}) - \mathbb{G}^\alpha_\omega(\boldsymbol{x},\boldsymbol{y}) \frac{\partial \overline{\mathbb{G}^\alpha_\omega}(\boldsymbol{y},\boldsymbol{z})}{\partial \nu} \right] d\sigma(\boldsymbol{y}) = 2i\Im m\{\mathbb{G}^\alpha_\omega(\boldsymbol{x},\boldsymbol{z})\}. \tag{2.23}$$

Proof. As both cases, $\alpha = p$ and $\alpha = s$, are similar, we only provide a proof for $\alpha = p$. For $\alpha = p$, indeed, we have

$$\begin{aligned}
&\int_{\partial\Omega} \left[\frac{\partial \mathbb{G}^p_\omega(\boldsymbol{x},\boldsymbol{y})}{\partial \nu} \overline{\mathbb{G}^p_\omega}(\boldsymbol{y},\boldsymbol{z}) - \mathbb{G}^p_\omega(\boldsymbol{x},\boldsymbol{y}) \frac{\partial \overline{\mathbb{G}^p_\omega}(\boldsymbol{y},\boldsymbol{z})}{\partial \nu} \right] d\sigma(\boldsymbol{y}) \\
&\qquad = [\mathcal{H}^p[-\delta_{\mathbf{0}}\mathbb{I}] * \overline{\mathbb{G}^p_\omega}(\cdot,\boldsymbol{z})](\boldsymbol{x}) - [\mathbb{G}^p_\omega(\boldsymbol{x},\cdot) * \mathcal{H}^p[-\delta_{\mathbf{0}}\mathbb{I}]](\boldsymbol{z}).
\end{aligned}$$

Using the fact that $\mathbb{G}^p_\omega(\boldsymbol{y},\boldsymbol{z}) = \mathbb{G}^p_{\omega,0}(\boldsymbol{y}-\boldsymbol{z}) = \mathbb{G}^p_{\omega,0}(\boldsymbol{z}-\boldsymbol{y})$, we can write

$$[\mathcal{H}^p[-\delta_{\mathbf{0}}\mathbb{I}] * \overline{\mathbb{G}^p_\omega}(\cdot,\boldsymbol{z})](\boldsymbol{x}) = [\mathcal{H}^p[-\delta_{\mathbf{0}}\mathbb{I}] * \overline{\mathbb{G}^p_{\omega,0}}(\cdot)](\boldsymbol{x}-\boldsymbol{z})$$

and

$$[\mathbb{G}^p_\omega(\boldsymbol{x},\cdot) * \mathcal{H}^p[-\delta_{\mathbf{0}}\mathbb{I}]](\boldsymbol{z}) = [\mathbb{G}^p_{\omega,0}(\cdot) * \mathcal{H}^p[-\delta_{\mathbf{0}}\mathbb{I}]](\boldsymbol{z}-\boldsymbol{x}) = [\mathcal{H}^p[-\delta_{\mathbf{0}}\mathbb{I}] * \mathbb{G}^p_{\omega,0}(\cdot)]](\boldsymbol{x}-\boldsymbol{z}).$$

Therefore,

$$\begin{aligned}\int_{\partial\Omega}\left[\frac{\partial\mathbb{G}^p_\omega(\boldsymbol{x},\boldsymbol{y})}{\partial\nu}\overline{\mathbb{G}^p_\omega}(\boldsymbol{y},\boldsymbol{z}) - \mathbb{G}^p_\omega(\boldsymbol{x},\boldsymbol{y})\frac{\partial\overline{\mathbb{G}^p_\omega}(\boldsymbol{y},\boldsymbol{z})}{\partial\nu}\right]d\sigma(\boldsymbol{y})&\\ = \mathcal{H}^p\left[2i\Im m\{\mathbb{G}^p_\omega(\boldsymbol{x},\boldsymbol{z})\}\right] = 2i\Im m\{\mathbb{G}^p_\omega(\boldsymbol{x},\boldsymbol{z})\},&\end{aligned}$$

where the last equality results from the fact that $\mathcal{H}^s\mathcal{H}^p = 0$. □

2.1.3 Approximation of the conormal derivative

In this subsection, we derive an approximation of the conormal derivative $\frac{\partial\mathbb{G}_\omega(\boldsymbol{x},\boldsymbol{y})}{\partial\nu}$, $\boldsymbol{y}\in\partial\Omega$, $\boldsymbol{x}\in\Omega$. In general this approximation involves the angles between the pressure and shear rays and the normal on $\partial\Omega$. This approximation becomes simple when Ω is a ball with very large radius, since in this case all rays are normal to $\partial\Omega$ (Proposition 2.4). It allows us to use a simplified version of the Helmholtz-Kirchhoff identity in order to analyze the imaging functional $\widetilde{\mathcal{I}}$ when Ω is a ball with large radius (Proposition 2.5).

Proposition 2.4. *If $\boldsymbol{n} = \widehat{\boldsymbol{y}-\boldsymbol{x}}$ and $|\boldsymbol{x}-\boldsymbol{y}| \gg 1$, then, for $\alpha = p, s$,*

$$\frac{\partial\mathbb{G}^\alpha_\omega(\boldsymbol{x},\boldsymbol{y})}{\partial\nu} = i\omega c_\alpha\mathbb{G}^\alpha_\omega(\boldsymbol{x},\boldsymbol{y}) + o\left(\frac{1}{|\boldsymbol{x}-\boldsymbol{y}|}\right). \tag{2.24}$$

Proof. It is enough to show that for all constant vectors $\boldsymbol{q}$,

$$\frac{\partial\mathbb{G}^p_\omega(\boldsymbol{x},\boldsymbol{y})\boldsymbol{q}}{\partial\nu} = i\omega c_p\mathbb{G}^p_\omega(\boldsymbol{x},\boldsymbol{y})\boldsymbol{q} + o\left(\frac{1}{|\boldsymbol{x}-\boldsymbol{y}|}\right)$$

and

$$\frac{\partial\mathbb{G}^s_\omega(\boldsymbol{x},\boldsymbol{y})\boldsymbol{q}}{\partial\nu} = i\omega c_s\mathbb{G}^s_\omega(\boldsymbol{x},\boldsymbol{y})\boldsymbol{q} + o\left(\frac{1}{|\boldsymbol{x}-\boldsymbol{y}|}\right).$$

Pressure component: Recall that

$$\mathbb{G}^p_\omega(\boldsymbol{x},\boldsymbol{y}) = -\frac{1}{\omega^2}\mathbb{D}G^p_\omega(\boldsymbol{x},\boldsymbol{y}) = \frac{1}{c_p^2}G^p_\omega(\boldsymbol{x},\boldsymbol{y})\widehat{\boldsymbol{y}-\boldsymbol{x}}\otimes\widehat{\boldsymbol{y}-\boldsymbol{x}} + o\left(\frac{1}{|\boldsymbol{x}-\boldsymbol{y}|}\right),$$

so we have

$$\mathbb{G}^p_\omega(\boldsymbol{x},\boldsymbol{y})\boldsymbol{q} = \frac{1}{c_p^2}G^p_\omega(\boldsymbol{x},\boldsymbol{y})\ (\widehat{\boldsymbol{y}-\boldsymbol{x}}\cdot\boldsymbol{q})\ \widehat{\boldsymbol{y}-\boldsymbol{x}} + o\left(\frac{1}{|\boldsymbol{x}-\boldsymbol{y}|}\right).$$

Therefore,

$$\begin{aligned}
\frac{\partial \mathbb{G}^p_\omega(\boldsymbol{x},\boldsymbol{y})\boldsymbol{q}}{\partial \nu} &= \lambda \nabla_{\boldsymbol{y}} \cdot (\mathbb{G}^p_\omega(\boldsymbol{x},\boldsymbol{y})\boldsymbol{q})\,\boldsymbol{n}(\boldsymbol{y}) + \mu\left[\nabla_{\boldsymbol{y}}(\mathbb{G}^p_\omega(\boldsymbol{x},\boldsymbol{y})\boldsymbol{q})^T + (\nabla_{\boldsymbol{y}}(\mathbb{G}^p_\omega(\boldsymbol{x},\boldsymbol{y})\boldsymbol{q})^T)^T\right]\boldsymbol{n}(\boldsymbol{y}) \\
&= \frac{\widehat{\boldsymbol{y}-\boldsymbol{x}}\cdot\boldsymbol{q}}{c_p^3} i\omega G^p_\omega(\boldsymbol{x},\boldsymbol{y})\left[\lambda\,\widehat{\boldsymbol{y}-\boldsymbol{x}}\cdot\widehat{\boldsymbol{y}-\boldsymbol{x}}\boldsymbol{n} + 2\mu(\widehat{\boldsymbol{y}-\boldsymbol{x}}\otimes\widehat{\boldsymbol{y}-\boldsymbol{x}})\boldsymbol{n}\right] + o\left(\frac{1}{|\boldsymbol{y}-\boldsymbol{x}|}\right) \\
&= \frac{\widehat{\boldsymbol{y}-\boldsymbol{x}}\cdot\boldsymbol{q}}{c_p^3} i\omega G^p_\omega(\boldsymbol{x},\boldsymbol{y})\left[\lambda\boldsymbol{n} + 2\mu(\widehat{\boldsymbol{y}-\boldsymbol{x}}\cdot\boldsymbol{n})\widehat{\boldsymbol{y}-\boldsymbol{x}}\right] + o\left(\frac{1}{|\boldsymbol{y}-\boldsymbol{x}|}\right) \\
&= \frac{\widehat{\boldsymbol{y}-\boldsymbol{x}}\cdot\boldsymbol{q}}{c_p^3} i\omega G^p_\omega(\boldsymbol{x},\boldsymbol{y})\left[\lambda\big(\boldsymbol{n}-\widehat{\boldsymbol{y}-\boldsymbol{x}}\big) + 2\mu\big(\widehat{\boldsymbol{y}-\boldsymbol{x}}\cdot\boldsymbol{n}-1\big)\widehat{\boldsymbol{y}-\boldsymbol{x}}\right] \\
&\quad + i\omega c_p \mathbb{G}^p_\omega(\boldsymbol{x},\boldsymbol{y})\boldsymbol{q} + o\left(\frac{1}{|\boldsymbol{y}-\boldsymbol{x}|}\right).
\end{aligned}$$

In particular, when $\boldsymbol{n} = \widehat{\boldsymbol{y}-\boldsymbol{x}}$, we have

$$\frac{\partial \mathbb{G}^p_\omega(\boldsymbol{x},\boldsymbol{y})\boldsymbol{q}}{\partial \nu} = i\omega c_p \mathbb{G}^p_\omega(\boldsymbol{x},\boldsymbol{y})\boldsymbol{q} + o\left(\frac{1}{|\boldsymbol{y}-\boldsymbol{x}|}\right).$$

Shear components: As

$$\mathbb{G}^s_\omega(\boldsymbol{x},\boldsymbol{y}) = \frac{1}{\omega^2}\left(\kappa_s^2\mathbb{I}+\mathbb{D}\right)G^s_\omega(\boldsymbol{x},\boldsymbol{y}) = \frac{1}{c_s^2}G^s_\omega(\boldsymbol{x},\boldsymbol{y})\left(\mathbb{I}-\widehat{\boldsymbol{y}-\boldsymbol{x}}\otimes\widehat{\boldsymbol{y}-\boldsymbol{x}}\right) + o\left(\frac{1}{|\boldsymbol{x}-\boldsymbol{y}|}\right),$$

we have

$$\mathbb{G}^s_\omega(\boldsymbol{x},\boldsymbol{y})\boldsymbol{q} = \frac{1}{c_s^2}G^s_\omega(\boldsymbol{x},\boldsymbol{y})\ \left(\boldsymbol{q}-(\widehat{\boldsymbol{y}-\boldsymbol{x}}\cdot\boldsymbol{q})\widehat{\boldsymbol{y}-\boldsymbol{x}}\right) + o\left(\frac{1}{|\boldsymbol{x}-\boldsymbol{y}|}\right).$$

Therefore,

$$\frac{\partial \mathbb{G}^s_\omega(\boldsymbol{x},\boldsymbol{y})\boldsymbol{q}}{\partial \nu} = \lambda \nabla_{\boldsymbol{y}} \cdot (\mathbb{G}^s_\omega(\boldsymbol{x},\boldsymbol{y})\boldsymbol{q})\,\boldsymbol{n}(\boldsymbol{y}) + \mu\left[\nabla_{\boldsymbol{y}}(\mathbb{G}^s_\omega(\boldsymbol{x},\boldsymbol{y})\boldsymbol{q})^T + (\nabla_{\boldsymbol{y}}(\mathbb{G}^s_\omega(\boldsymbol{x},\boldsymbol{y})\boldsymbol{q})^T)^T\right]\boldsymbol{n}(\boldsymbol{y}).$$

Now, remark that

$$\begin{aligned}
\lambda\nabla.(\mathbb{G}^s_\omega(\boldsymbol{x},\boldsymbol{y})\boldsymbol{q})\,\boldsymbol{n} &= \lambda\frac{i\omega}{c_s^3}G^s_\omega(\boldsymbol{x},\boldsymbol{y})\left[\left(\boldsymbol{q}-(\widehat{\boldsymbol{y}-\boldsymbol{x}}\cdot\boldsymbol{q})\widehat{\boldsymbol{y}-\boldsymbol{x}}\right)\cdot\widehat{\boldsymbol{y}-\boldsymbol{x}}\right]\boldsymbol{n} + o\left(\frac{1}{|\boldsymbol{x}-\boldsymbol{y}|}\right) \\
&= o\left(\frac{1}{|\boldsymbol{x}-\boldsymbol{y}|}\right),
\end{aligned}$$

and

$$\begin{aligned}
&\mu\left[\nabla\mathbb{G}^s_\omega(\boldsymbol{x},\boldsymbol{y})\boldsymbol{q} + \nabla\mathbb{G}^s_\omega(\boldsymbol{x},\boldsymbol{y})\boldsymbol{q}^T\right]\boldsymbol{n} \\
&= \mu\frac{i\omega}{c_s^3}G^s_\omega(\boldsymbol{x},\boldsymbol{y})\left[\boldsymbol{q}\otimes\widehat{\boldsymbol{y}-\boldsymbol{x}} + \widehat{\boldsymbol{y}-\boldsymbol{x}}\otimes\boldsymbol{q} - 2(\widehat{\boldsymbol{y}-\boldsymbol{x}}\cdot\boldsymbol{q})\widehat{\boldsymbol{y}-\boldsymbol{x}}\otimes\widehat{\boldsymbol{y}-\boldsymbol{x}}\right]\boldsymbol{n} + o\left(\frac{1}{|\boldsymbol{x}-\boldsymbol{y}|}\right) \\
&= \mu\frac{i\omega}{c_s^3}G^s_\omega(\boldsymbol{x},\boldsymbol{y})\left[(\widehat{\boldsymbol{y}-\boldsymbol{x}}\cdot\boldsymbol{n})\boldsymbol{q} + (\boldsymbol{q}\cdot\boldsymbol{n})\widehat{\boldsymbol{y}-\boldsymbol{x}} - 2(\widehat{\boldsymbol{y}-\boldsymbol{x}}\cdot\boldsymbol{q})(\widehat{\boldsymbol{y}-\boldsymbol{x}}\cdot\boldsymbol{n})\widehat{\boldsymbol{y}-\boldsymbol{x}}\right] + o\left(\frac{1}{|\boldsymbol{x}-\boldsymbol{y}|}\right) \\
&= \mu\frac{i\omega}{c_s^3}G^s_\omega(\boldsymbol{x},\boldsymbol{y})\left[(\widehat{\boldsymbol{y}-\boldsymbol{x}}\cdot\boldsymbol{n})-1\right]\left[\boldsymbol{q}-(\widehat{\boldsymbol{y}-\boldsymbol{x}}\cdot\boldsymbol{q})\widehat{\boldsymbol{y}-\boldsymbol{x}}\right] \\
&\quad + \mu\frac{i\omega}{c_s^3}G^s_\omega(\boldsymbol{x},\boldsymbol{y})\left[\left(\boldsymbol{q}\cdot\boldsymbol{n}-(\widehat{\boldsymbol{y}-\boldsymbol{x}}\cdot\boldsymbol{q})(\widehat{\boldsymbol{y}-\boldsymbol{x}}\cdot\boldsymbol{n})\right)\widehat{\boldsymbol{y}-\boldsymbol{x}}\right] i\omega c_s\mathbb{G}^s_\omega(\boldsymbol{x},\boldsymbol{y}) + o\left(\frac{1}{|\boldsymbol{x}-\boldsymbol{y}|}\right).
\end{aligned}$$

In particular, when $\boldsymbol{n} = \widehat{\boldsymbol{y}-\boldsymbol{x}}$, we have

$$\frac{\partial \mathbb{G}^s_\omega(\boldsymbol{x},\boldsymbol{y})\boldsymbol{q}}{\partial \nu} = i\omega c_s \mathbb{G}^s_\omega(\boldsymbol{x},\boldsymbol{y})\boldsymbol{q} + o\left(\frac{1}{|\boldsymbol{y}-\boldsymbol{x}|}\right).$$

□

The following is a direct consequence of Propositions 2.2, 2.3, and 2.4.

Proposition 2.5. *Let $\Omega \subset \mathbb{R}^d$ be a ball with radius R. Then, for all $\boldsymbol{x}, \boldsymbol{z} \in \Omega$ sufficiently far from the boundary $\partial\Omega$, we have*

$$\Re e\left\{\int_{\partial\Omega} \mathbb{G}^\alpha_\omega(\boldsymbol{x},\boldsymbol{y})\overline{\mathbb{G}^\alpha_\omega}(\boldsymbol{y},\boldsymbol{z})d\sigma(\boldsymbol{y})\right\} \simeq \frac{1}{\omega c_\alpha}\Im m\{\mathbb{G}^\alpha_\omega(\boldsymbol{x},\boldsymbol{z})\}, \qquad \alpha = p, s, \quad (2.25)$$

$$\Re e\left\{\int_{\partial\Omega} \mathbb{G}^s_\omega(\boldsymbol{x},\boldsymbol{y})\overline{\mathbb{G}^p_\omega}(\boldsymbol{y},\boldsymbol{z})d\sigma(\boldsymbol{y})\right\} \simeq 0. \quad (2.26)$$

2.1.4 Analysis of the imaging functional $\widetilde{\mathcal{I}}$

In this subsection, we assume that Ω is a ball of radius R in $\mathbb{R}^d$ and that the support, $supp\{\mathbf{F}\}$, of $\mathbf{F}$ is sufficiently localized at the center of Ω so that for all $\boldsymbol{x} \in supp\{\mathbf{F}\}$ and for all $\boldsymbol{y} \in \partial\Omega$

$$\widehat{\boldsymbol{y}-\boldsymbol{x}} = \boldsymbol{n}(\boldsymbol{y}) + o\left(\frac{1}{|\boldsymbol{y}-\boldsymbol{x}|}\right).$$

Then, we have the following theorem.

Theorem 2.6. *Let $\boldsymbol{x} \in \Omega$ be sufficiently far from the boundary $\partial\Omega$ and $\widetilde{\mathcal{I}}$ be defined by (2.7). Then,*

$$\widetilde{\mathcal{I}}(\boldsymbol{x}) \simeq \mathbf{F}(\boldsymbol{x}). \quad (2.27)$$

Proof. From (2.18) we have

$$\widetilde{\mathcal{I}}(\boldsymbol{x}) = \frac{1}{4\pi}\int_{\mathbb{R}^d}\int_{\mathbb{R}} \omega^2 \left[\int_{\partial\Omega} \widetilde{\mathbb{G}}_\omega(\boldsymbol{x},\boldsymbol{y})\overline{\mathbb{G}}_\omega(\boldsymbol{y},\boldsymbol{z}) + \overline{\widetilde{\mathbb{G}}}_\omega(\boldsymbol{x},\boldsymbol{y})\mathbb{G}_\omega(\boldsymbol{y},\boldsymbol{z})\, d\sigma(\boldsymbol{y})\right] d\omega \mathbf{F}(\boldsymbol{z})\, d\boldsymbol{z},$$

where

$$\widetilde{\mathbb{G}}_\omega(\boldsymbol{x},\boldsymbol{y}) = c_s\mathbb{G}^s_\omega(\boldsymbol{x},\boldsymbol{y}) + c_p\mathbb{G}^p_\omega(\boldsymbol{x},\boldsymbol{y}).$$

Proposition 2.5 allows us to write

$$\begin{aligned}\widetilde{\mathcal{I}}(\boldsymbol{x}) &\simeq \frac{1}{4\pi}\int_{\mathbb{R}^d}\int_{\mathbb{R}} \omega^2 \left[\int_{\partial\Omega} \widetilde{\mathbb{G}}_\omega(\boldsymbol{x},\boldsymbol{y})\overline{\mathbb{G}}_\omega(\boldsymbol{y},\boldsymbol{z}) + \overline{\mathbb{G}}_\omega(\boldsymbol{x},\boldsymbol{y})\widetilde{\mathbb{G}}_\omega(\boldsymbol{y},\boldsymbol{z})\, d\sigma(\boldsymbol{y})\right] d\omega \mathbf{F}(\boldsymbol{z})\, d\boldsymbol{z} \\ &\simeq \frac{1}{4\pi}\int_{\mathbb{R}^d}\int_{\mathbb{R}} \omega^2 \left[\int_{\partial\Omega} \widetilde{\mathbb{G}}_\omega(\boldsymbol{x},\boldsymbol{y})\overline{\mathbb{G}}_\omega(\boldsymbol{y},\boldsymbol{z}) + \mathbb{G}_\omega(\boldsymbol{x},\boldsymbol{y})\overline{\widetilde{\mathbb{G}}}_\omega(\boldsymbol{y},\boldsymbol{z})\, d\sigma(\boldsymbol{y})\right] d\omega \mathbf{F}(\boldsymbol{z})\, d\boldsymbol{z}.\end{aligned}$$

Proposition 2.4 then gives

$$\begin{aligned}\widetilde{\mathcal{I}}(\boldsymbol{x}) &\simeq \frac{1}{4\pi}\int_{\mathbb{R}^d}\int_{\mathbb{R}} -i\omega \left[\frac{\partial \mathbb{G}_\omega(\boldsymbol{x},\boldsymbol{y})}{\partial\nu}\overline{\mathbb{G}}_\omega(\boldsymbol{y},\boldsymbol{z}) - \mathbb{G}_\omega(\boldsymbol{x},\boldsymbol{y})\frac{\partial\overline{\mathbb{G}}_\omega(\boldsymbol{y},\boldsymbol{z})}{\partial\nu}\right] d\omega \mathbf{F}(\boldsymbol{z})\, d\boldsymbol{z} \\ &\simeq \frac{1}{2\pi}\int_{\mathbb{R}^d}\int_{\mathbb{R}} \omega\Im m\left[\mathbb{G}_\omega(\boldsymbol{x},\boldsymbol{z})\right] d\omega \mathbf{F}(\boldsymbol{z})\, d\boldsymbol{z} \simeq \mathbf{F}(\boldsymbol{x}).\end{aligned}$$

The last approximation results from the identity

$$\frac{1}{2\pi}\int_{\mathbb{R}} -i\omega\mathbb{G}_\omega(\boldsymbol{x},\boldsymbol{z})d\omega = \delta_{\boldsymbol{x}}(\boldsymbol{z})\mathbb{I},$$

which comes from the integration of the time-dependent version of (2.9) between $t = 0^-$ and $t = 0^+$. □

If the unweighted time-reversal imaging function $\mathcal{I}$ is used instead of $\widetilde{\mathcal{I}}$, then crossed terms remain. Using the same arguments as above we find

$$\begin{aligned}\mathcal{I}(\boldsymbol{x}) &\simeq \frac{c_s+c_p}{c_s c_p}\frac{1}{4\pi}\int_{\mathbb{R}^d}\int_{\mathbb{R}} \omega\Im m\left[(\mathbb{G}^p_\omega+\mathbb{G}^s_\omega)(\boldsymbol{x},\boldsymbol{z})\right]d\omega\mathbf{F}(\boldsymbol{z})\,d\boldsymbol{z}\\ &\quad+\frac{c_s-c_p}{c_s c_p}\frac{1}{4\pi}\int_{\mathbb{R}^d}\int_{\mathbb{R}} \omega\Im m\left[(\mathbb{G}^p_\omega-\mathbb{G}^s_\omega)(\boldsymbol{x},\boldsymbol{z})\right]d\omega\mathbf{F}(\boldsymbol{z})\,d\boldsymbol{z}\\ &\simeq \frac{c_s+c_p}{2c_s c_p}\mathbf{F}(\boldsymbol{x})+\frac{c_s-c_p}{2c_s c_p}\int_{\mathbb{R}^d}\mathbb{B}(\boldsymbol{x},\boldsymbol{z})\mathbf{F}(\boldsymbol{z})d\boldsymbol{z}, \end{aligned} \tag{2.28}$$

where

$$\mathbb{B}(\boldsymbol{x},\boldsymbol{z}) = \frac{1}{2\pi}\int_{\mathbb{R}} \omega\Im m\left[(\mathbb{G}^p_\omega-\mathbb{G}^s_\omega)(\boldsymbol{x},\boldsymbol{z})\right]d\omega \tag{2.29}$$

is the operator that describes the error in the reconstruction of the source $\mathbf{F}$ obtained with $\mathcal{I}$ when $c_s \neq c_p$. In particular the operator $\mathbb{B}$ is not diagonal, which means that the reconstruction mixes the components of $\mathbf{F}$.

2.2 Numerical simulations

Here we present numerical illustrations and describe our algorithms for numerical resolution of the source problem to show that $\widetilde{\mathcal{I}}$ provides a better reconstruction than $\mathcal{I}$.

2.2.1 Description of the algorithm

We describe the algorithm we used for the numerical resolution of the elastic wave equation in 2D:

$$\begin{cases} \dfrac{\partial^2\mathbf{u}}{\partial t^2}(\boldsymbol{x},t) = \left[\mu\Delta\mathbf{u}+(\lambda+\mu)\nabla(\nabla\cdot\mathbf{u})\right](\boldsymbol{x},t), \qquad (\boldsymbol{x},t)\in\mathbb{R}^2\times\mathbb{R},\\ \mathbf{u}(\boldsymbol{x},0)=\mathbf{F}(\boldsymbol{x}) \quad \text{and} \quad \dfrac{\partial\mathbf{u}}{\partial t}(\boldsymbol{x},0)=\mathbf{0}. \end{cases} \tag{2.30}$$

This equation is computed on the box $Q = [-L/2, L/2]^2$ such that $\Omega \subset Q$ with periodic boundary conditions. We use a *splitting spectral Fourier* approach [15] coupled with a perfectly matched layer (PML) technique [22] to simulate a free outgoing interface on ∂Q.

With the notation $\mathbf{u} = (u_1, u_2)$ and $\boldsymbol{x} = (x_1, x_2)$, the elastic wave equation can be rewritten as a first order partial differential equation:

$$\partial_t P = AP + BP,$$

where

$$P = \begin{pmatrix} u_1 \\ \partial_t u_1 \\ u_2 \\ \partial_t u_2 \end{pmatrix}, \quad A = \begin{pmatrix} 0 & 1 & 0 & 0 \\ (\lambda+2\mu)\partial_{x_1}^2 + \mu\partial_{x_2}^2 & 0 & 0 & 0 \\ 0 & 0 & 0 & 1 \\ 0 & 0 & (\lambda+2\mu)\partial_{x_2}^2 + \mu\partial_{x_1}^2 & 0 \end{pmatrix},$$

and

$$B = \begin{pmatrix} 0 & 0 & 0 & 0 \\ 0 & 0 & (\lambda+\mu)\partial_{x_1}\partial_{x_2} & 0 \\ 0 & 0 & 0 & 0 \\ (\lambda+\mu)\partial_{x_1}\partial_{x_2} & 0 & 0 & 0 \end{pmatrix}.$$

This equation is integrated via *Strang's splitting method* [32]. This splitting approach is known to be of order 2 and reads

$$\exp(-t(A+B)) = \exp(-t/2B)\,\exp(-tA)\,\exp(-t/2B) + o(t^2).$$

The first operator A is then computed exactly in the spatial Fourier space. Indeed, the Fourier transform of $P_A(\boldsymbol{x},t)\exp(-At)P(\boldsymbol{x})$ satisfies

$$\begin{cases} \widehat{u_{A,1}}(\boldsymbol{\xi},t) & = \cos\left(\sqrt{\xi^2_{\lambda,\mu,1}}t\right)\widehat{u_1}(\boldsymbol{\xi}) + t\ \mathrm{sinc}\left(\sqrt{\xi^2_{\lambda,\mu,1}}t\right)\widehat{\partial_t u_1}(\boldsymbol{\xi}), \\ \widehat{\partial_t u_{A,1}}(\boldsymbol{\xi},t) & = \cos\left(\sqrt{\xi^2_{\lambda,\mu,1}}t\right)\widehat{\partial_t u_1}(\boldsymbol{\xi}) - \sqrt{\xi^2_{\lambda,\mu,1}}\sin\left(\sqrt{\xi^2_{\lambda,\mu,1}}t\right)\widehat{u_1}(\boldsymbol{\xi}), \\ \widehat{u_{A,2}}(\boldsymbol{\xi},t) & = \cos\left(\sqrt{\xi^2_{\lambda,\mu,2}}t\right)\widehat{u_2}(\boldsymbol{\xi}) + t\ \mathrm{sinc}\left(\sqrt{\xi^2_{\lambda,\mu,2}}t\right)\widehat{\partial_t u_2}(\boldsymbol{\xi}), \\ \widehat{\partial_t u_{A,2}}(\boldsymbol{\xi},t) & = \cos\left(\sqrt{\xi^2_{\lambda,\mu,2}}t\right)\widehat{\partial_t u_2}(\boldsymbol{\xi}) - \sqrt{\xi^2_{\lambda,\mu,2}}\sin\left(\sqrt{\xi^2_{\lambda,\mu,2}}t\right)\widehat{u_2}(\boldsymbol{\xi}), \end{cases}$$

with

$$\xi^2_{\lambda,\mu,1} = 4\pi^2(\lambda+2\mu)\xi_1^2 + \mu\xi_2^2, \quad \xi^2_{\lambda,\mu,2} = 4\pi^2(\lambda+2\mu)\xi_2^2 + \mu\xi_1^2, \quad \text{and} \quad \mathrm{sinc}(t) = \sin(t)/t.$$

The second operator B is also integrated exactly. We have

$$P_B(\boldsymbol{x},t) = \exp(-Bt)P(\boldsymbol{x}) = \begin{pmatrix} u_1(\boldsymbol{x}) \\ \partial_t u_1(\boldsymbol{x}) - t\,(\lambda+\mu)\,\partial_{x_1}\partial_{x_2}u_2(\boldsymbol{x}) \\ u_2(\boldsymbol{x}) \\ \partial_t u_2(\boldsymbol{x}) - t\,(\lambda+\mu)\,\partial_{x_1}\partial_{x_2}u_1(\boldsymbol{x}) \end{pmatrix}.$$

This global algorithm appears to be stable under a classical condition of the form

$$\delta_t \leq c(\lambda,\mu)\delta_x^2,$$

where δ_t and δ_x denote respectively the time and the spatial step of discretization. Here $c(\lambda,\mu)$ is a constant which depends only on Lamé coefficients λ and μ.

The functional $\widetilde{\mathcal{I}}(\boldsymbol{x})$ requires also a Helmholtz decomposition algorithm. As the support of the function $\widetilde{\mathcal{I}}(\boldsymbol{x})$ is included in $\Omega \subset Q$, we apply a Dirichlet boundary condition on ∂Q. This decomposition is numerically obtained with a fast algorithm [37] based on a symmetry principle and a Fourier-Helmholtz decomposition algorithm.

2.2.2 Experiments

In the sequel, for numerical illustrations, Ω is taken as a unit disc. Its boundary is discretized by 1024 sensors. Each solution of elastic wave equation is computed over $(\boldsymbol{x}, t) \in [-L/2, L/2]^2 \times [0, T]$ with $L = 4$ and $T = 2$. We use a step of discretization given by $dt = T/2^{13}$ and $dx = L/2^9$.

Figure 1 presents a first experiment with Lamé parameters $(\lambda, \mu) = (1, 1)$. The first (top) line corresponds to the 2 components of the initial source $\mathbf{F}$. The second line corresponds to the data $\mathbf{g}(\boldsymbol{y}, t) = \mathbf{u}(\boldsymbol{y}, t)$ recorded over $(\boldsymbol{y}, t) \in \partial\Omega \times [0, T]$. Note that the shear and pressure waves are mixed in the recorded signal and it seems difficult to separate them. The third line corresponds to the imaging functional $\mathcal{I}(\boldsymbol{x})$. This example clearly shows that the reconstruction of the source $\mathbf{F}$ is not so accurate with classical time-reversal imaging. Moreover, in the last row, the plots represent the modified imaging functional $\widetilde{\mathcal{I}}(\boldsymbol{x})$ where the reconstruction is quite better and nearly optimal.

Figure 2 shows another example with different Lamé parameters $(\lambda, \mu) = (10, 1)$. The same conclusion holds.

In Figure 3, we use a "less localized" (large) source distribution. We observe some artifacts in the reconstruction of the imaging functional $\widetilde{\mathcal{I}}$. We can also observe, from the recorded data, that the pressure and shear waves are very much "mixed" with each other. We expect that the artifacts in the reconstruction are the consequence of such mixing. In this situation, we do not have a real orthogonality between the two waves on $\partial\Omega$.

To conclude, $\widetilde{\mathcal{I}}$ provides a better reconstruction of the sources than $\mathcal{I}$. However, in certain cases, the reconstructions by $\widetilde{\mathcal{I}}$ are not optimal, and need further improvements.

3 Time-reversal algorithm for viscoelastic media

In this section, we investigate the source inverse problem in an elastic attenuating medium. We provide an efficient regularized time-reversal imaging algorithm which corrects for the leading-order terms of the attenuation effect. Consider the viscoelastic wave equation in a open medium $\Omega \subset \mathbb{R}^d$ with $d = 2, 3$, *i.e.*,

$$\begin{cases} \dfrac{\partial^2 \mathbf{u}_a}{\partial t^2}(\boldsymbol{x}, t) - \mathcal{L}_{\lambda,\mu}\mathbf{u}_a(\boldsymbol{x}, t) - \dfrac{\partial}{\partial t}\mathcal{L}_{\eta_\lambda,\eta_\mu}\mathbf{u}_a(\boldsymbol{x}, t) = \dfrac{d\delta_0(t)}{dt}\mathbf{F}(\boldsymbol{x}), & (\boldsymbol{x}, t) \in \mathbb{R}^d \times \mathbb{R}, \\ \mathbf{u}_a(\boldsymbol{x}, t) = \dfrac{\partial \mathbf{u}_a}{\partial t}(\boldsymbol{x}, t) = \mathbf{0}, & t < 0, \end{cases} \tag{3.1}$$

where the viscosity parameters η_μ and η_λ are positive constants and account for losses in the medium.

As in the acoustic case [4], the strategy of time reversal is to consider the functional

$$\mathcal{I}_a(\boldsymbol{x}) = \int_0^T \mathbf{v}_{s,a}(\boldsymbol{x}, T)ds, \tag{3.2}$$

where $\mathbf{v}_{s,a}$ should be the *solution* of the adjoint (time-reversed) viscoelastic wave equation,

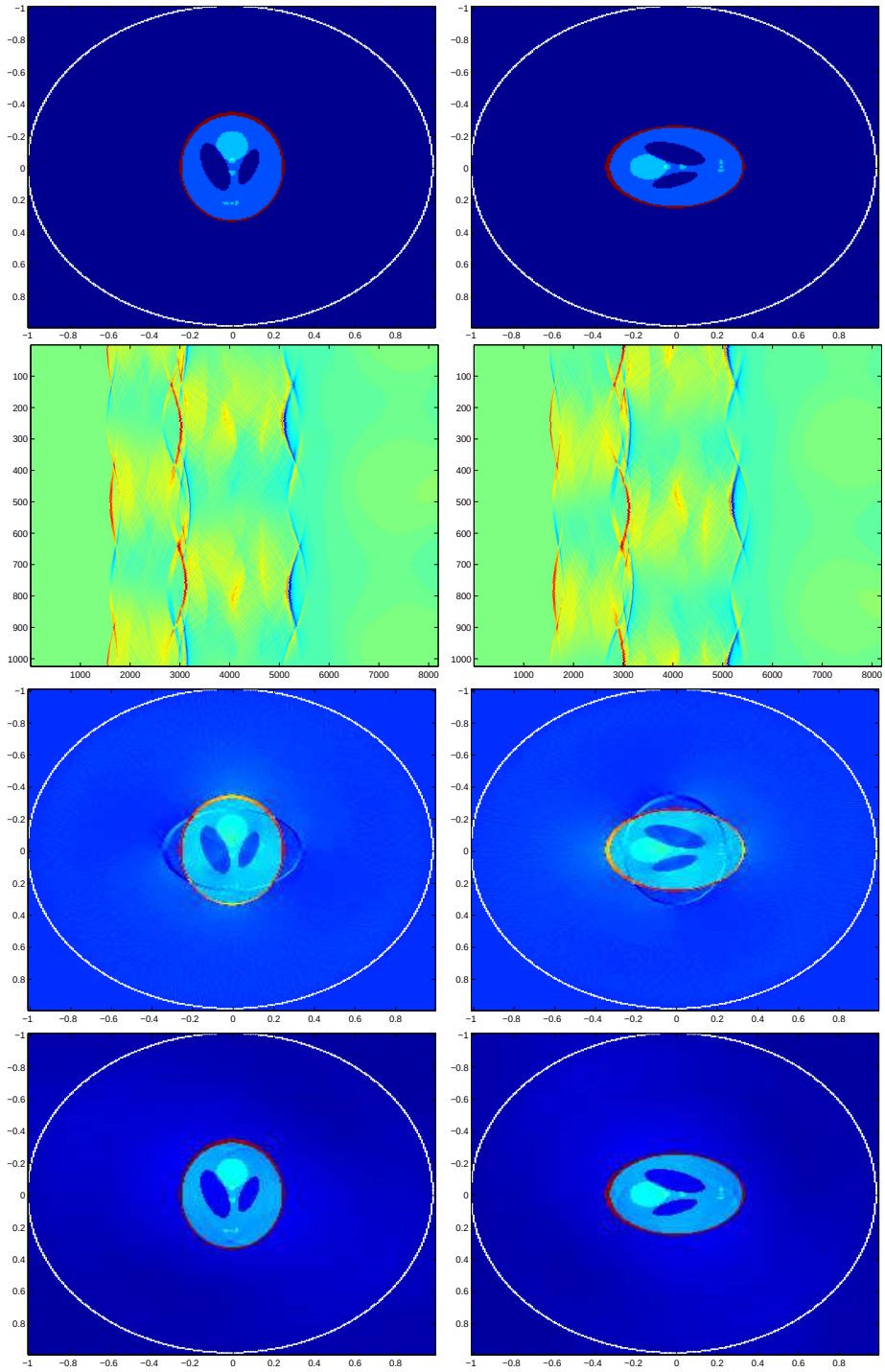

Figure 1: Test 1: Source reconstruction; Comparison between the imaging functionals $\mathcal{I}$ and $\widetilde{\mathcal{I}}$ with Lamé constants $(\lambda, \mu) = (1, 1)$. From top to bottom: First line: the source $\mathbf{F}$; Second line: recorded data $\mathbf{g}(\boldsymbol{y}, t)$; Third line: imaging functional $\mathcal{I}$; Last line: imaging functional $\widetilde{\mathcal{I}}$.

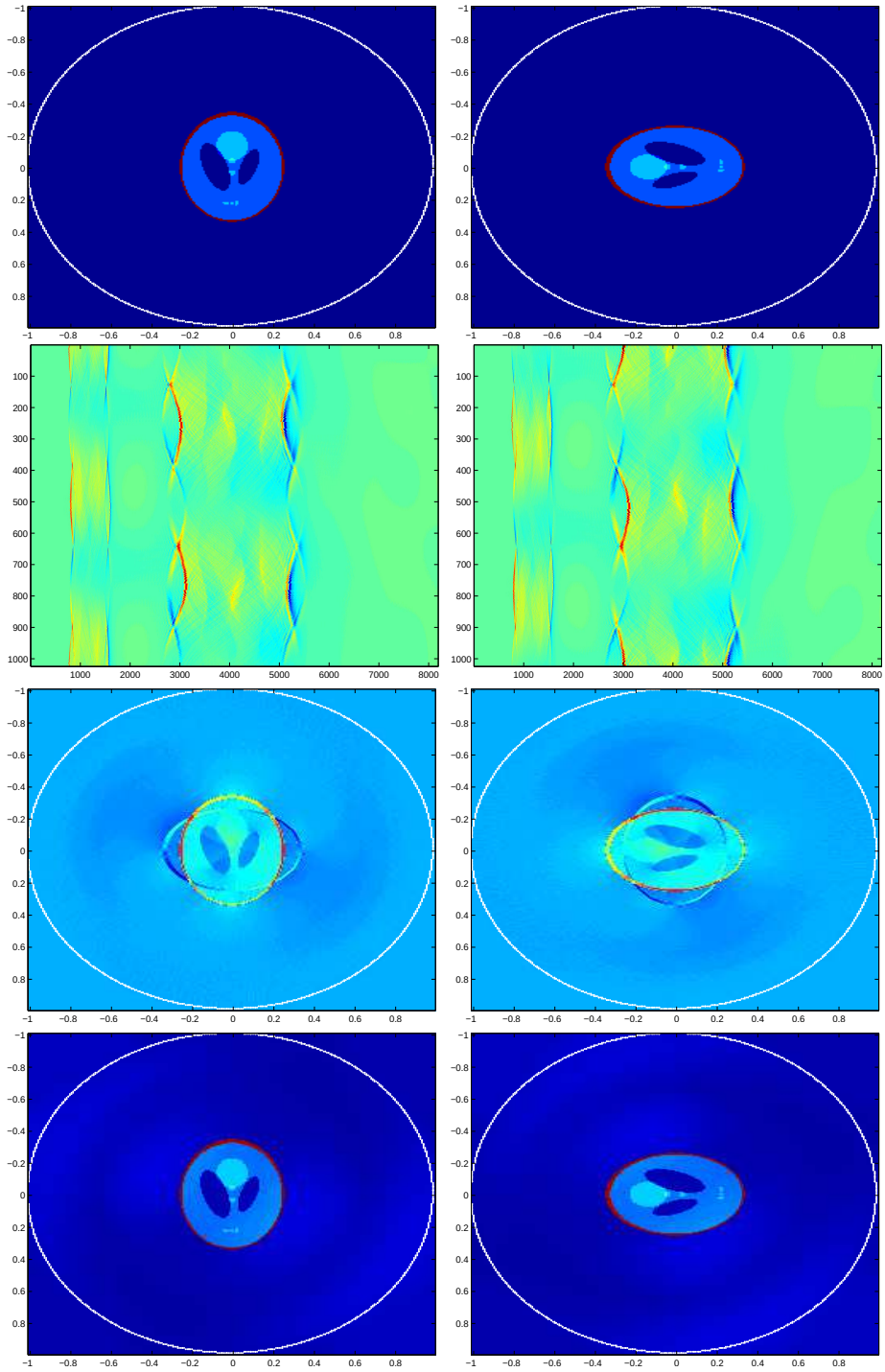

Figure 2: Test 2: Source reconstruction; Comparison between the imaging functionals $\mathcal{I}$ and $\widetilde{\mathcal{I}}$ with Lamé constants $(\lambda, \mu) = (10, 1)$; First line: the source $\mathbf{F}$; Second line: recorded data $\mathbf{g}(\boldsymbol{y}, t)$; Third line: imaging functional $\mathcal{I}$; Last line: imaging functional $\widetilde{\mathcal{I}}$.

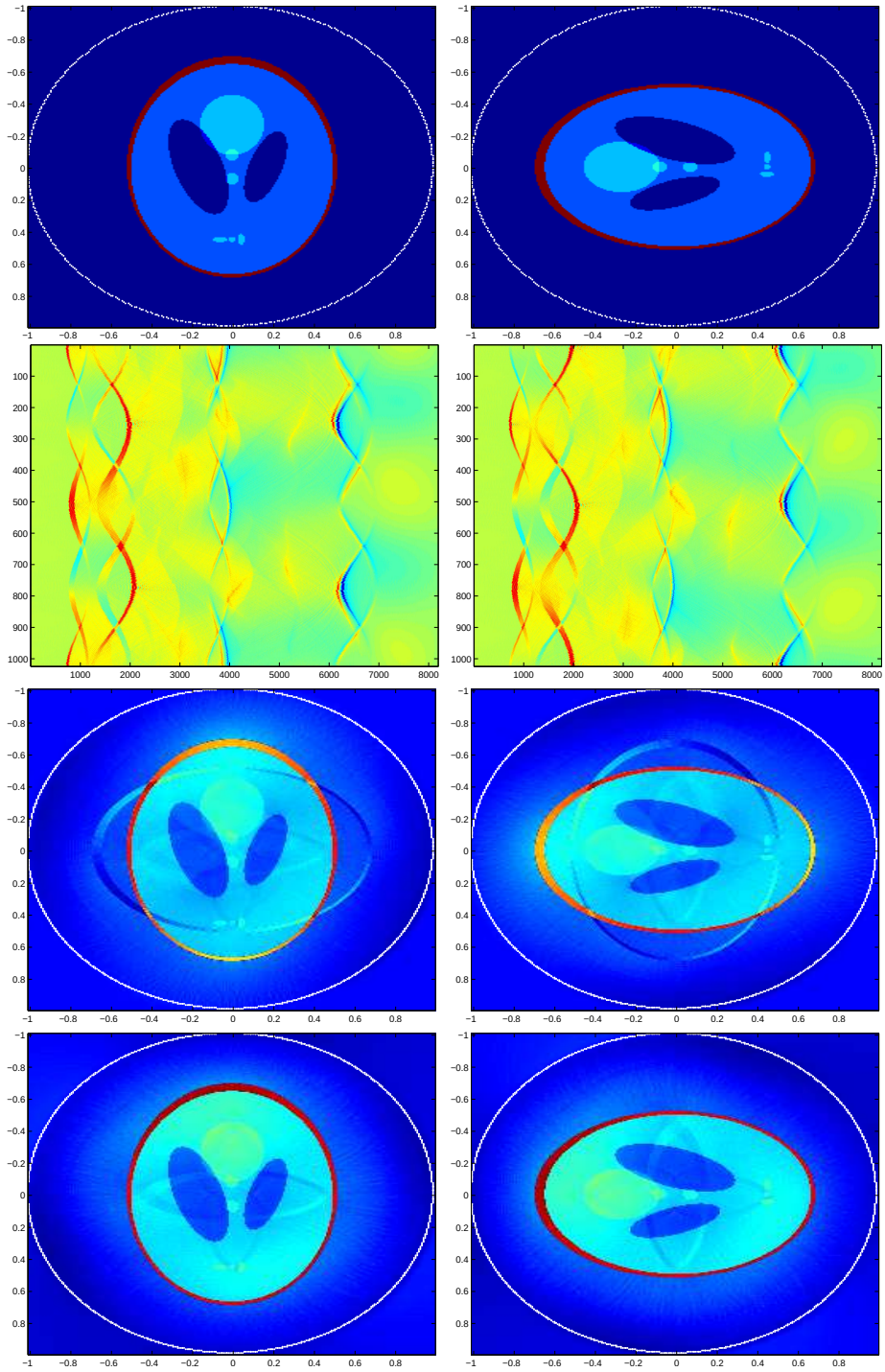

Figure 3: Test 3: Source reconstruction; Comparison between the imaging functionals $\mathcal{I}$ and $\widetilde{\mathcal{I}}$ with Lamé constants $(\lambda, \mu) = (1, 1)$ and less localized source than in Figure 1; First line: the source $\mathbf{F}$; Second line: recorded data $\mathbf{g}(\boldsymbol{y}, t)$; Third line: imaging functional $\mathcal{I}$; Last line: imaging functional $\widetilde{\mathcal{I}}$.

i.e.,

$$\begin{cases} \dfrac{\partial^2 \mathbf{v}_{s,a}}{\partial t^2}(\boldsymbol{x},t) - \mathcal{L}_{\lambda,\mu}\mathbf{v}_{s,a}(\boldsymbol{x},t) \\ \qquad\qquad + \dfrac{\partial}{\partial t}\mathcal{L}_{\eta_\lambda,\eta_\mu}\mathbf{v}_{s,a}(\boldsymbol{x},t) = \dfrac{d\delta_s(t)}{dt}\mathbf{g}_a(\boldsymbol{x},T-s)\delta_{\partial\Omega}(\boldsymbol{x}), & (\boldsymbol{x},t)\in\mathbb{R}^d\times\mathbb{R}, \\ \mathbf{v}_s(\boldsymbol{x},t) = \dfrac{\partial \mathbf{v}_s}{\partial t}(\boldsymbol{x},t) = \mathbf{0} & \boldsymbol{x}\in\mathbb{R}^d, t<s. \end{cases} \tag{3.3}$$

Further, the idea is to enhance image resolution using $\widetilde{\mathcal{I}}_a$, as in purely elastic media, where

$$\widetilde{\mathcal{I}}_a = c_s\mathcal{H}^s\left[\mathcal{I}_a\right] + c_p\mathcal{H}^p\left[\mathcal{I}_a\right].$$

Unfortunately, the adjoint viscoelastic problem is severely ill-posed. Indeed, the frequency component is exponentially increasing due to the presence of the *anti-damping* term $\left(+\partial_t\mathcal{L}_{\eta_\lambda,\eta_\mu}\mathbf{v}_{s,a}\right)$, which induces instability. Therefore, we need to regularize the adjoint problem by truncating high-frequency components either in time or in space.

Let us introduce the outgoing Green's tensor $\mathbb{G}_{a,\omega}$ associated to the viscoelastic wave equation

$$(\mathcal{L}_{\lambda,\mu} - i\omega\mathcal{L}_{\eta_\lambda,\eta_\mu} + \omega^2)\mathbb{G}_{a,\omega}(\boldsymbol{x},\boldsymbol{y}) = -\delta_{\boldsymbol{y}}(\boldsymbol{x})\mathbb{I}, \qquad \boldsymbol{x},\boldsymbol{y}\in\mathbb{R}^d, \tag{3.4}$$

and let $\mathbb{G}_{-a,\omega}$ be the *adjoint* viscoelastic Green's tensor, that is, the solution to

$$(\mathcal{L}_{\lambda,\mu} + i\omega\mathcal{L}_{\eta_\lambda,\eta_\mu} + \omega^2)\mathbb{G}_{-a,\omega}(\boldsymbol{x},\boldsymbol{y}) = -\delta_{\boldsymbol{y}}(\boldsymbol{x})\mathbb{I}, \qquad \boldsymbol{x},\boldsymbol{y}\in\mathbb{R}^d. \tag{3.5}$$

We introduce an approximation $\mathbf{v}_{s,a,\rho}$ of the adjoint wave $\mathbf{v}_{s,a}$ by

$$\mathbf{v}_{s,a,\rho}(\boldsymbol{x},t) = -\frac{1}{2\pi}\int_{|\omega|\le\rho}\left\{\int_{\partial\Omega} i\omega\mathbb{G}_{-a,\omega}(\boldsymbol{x},\boldsymbol{y})\mathbf{g}_a(\boldsymbol{y},T-s)d\sigma(\boldsymbol{y})\right\}\exp\left(-i\omega(t-s)\right)d\omega, \tag{3.6}$$

where $\rho\in\mathbb{R}^+$ is the cut-off parameter. The regularized time-reversal imaging functional defined by

$$\mathcal{I}_{a,\rho}(\boldsymbol{x}) = \int_0^T \mathbf{v}_{s,a,\rho}(\boldsymbol{x},T)ds, \tag{3.7}$$

can be written as

$$\mathcal{I}_{a,\rho}(\boldsymbol{x}) = \int_{\partial\Omega}\int_0^T \frac{\partial}{\partial t}\mathbb{G}_{-a,\rho}(\boldsymbol{x},\boldsymbol{y},T-s)\mathbf{g}_a(\boldsymbol{y},T-s)ds\,d\sigma(\boldsymbol{y}), \tag{3.8}$$

where

$$\mathbb{G}_{-a,\rho}(\boldsymbol{x},\boldsymbol{y},t) = \frac{1}{2\pi}\int_{|\omega|\le\rho}\mathbb{G}_{-a,\omega}(\boldsymbol{x},\boldsymbol{y})\exp\left(-i\omega t\right)\,d\omega. \tag{3.9}$$

Remark 3.1. *Let $\mathcal{S}'$ be the space of tempered distributions,* i.e.*, the dual of the Schwartz space $\mathcal{S}$ of rapidly decreasing functions [23]. The function $\mathbf{v}_{s,a,\rho}(\boldsymbol{x},t)$ can be identified as the solution of the following wave equation:*

$$\frac{\partial^2 \mathbf{v}_{s,a,\rho}}{\partial t^2}(\boldsymbol{x},t) - \mathcal{L}_{\lambda,\mu}\mathbf{v}_{s,a,\rho}(\boldsymbol{x},t) + \frac{\partial}{\partial t}\mathcal{L}_{\eta_\lambda,\eta_\mu}\mathbf{v}_{s,a,\rho}(\boldsymbol{x},t) = S_\rho\left[\frac{d\delta_s(t)}{dt}\right]\mathbf{g}_a(\boldsymbol{x},T-s)\delta_{\partial\Omega}(\boldsymbol{x}), \tag{3.10}$$

where the operator S_ρ is defined on the space $\mathcal{S}'$ by

$$S_\rho\left[\psi\right](t) = \frac{1}{2\pi}\int_{|\omega|\leq\rho} \exp\left(-i\omega t\right)\hat{\psi}(\omega)d\omega, \tag{3.11}$$

with

$$\hat{\psi}(\omega) = \int_{\mathbb{R}} \psi(t)\exp(i\omega t)\,dt. \tag{3.12}$$

3.1 Green's tensor in viscoelastic media

As in Section 2, we decompose $\mathbb{G}_{\pm a,\omega}$ in the form

$$\mathbb{G}_{\pm a,\omega} = \mathbb{G}^s_{\pm a,\omega} + \mathbb{G}^p_{\pm a,\omega}, \tag{3.13}$$

where $\mathbb{G}^s_{\pm a,\omega}$ and $\mathbb{G}^p_{\pm a,\omega}$ are respectively the fundamental solutions of

$$(\mathcal{L}_{\lambda,\mu} \mp i\omega\mathcal{L}_{\eta_\lambda,\eta_\mu} + \omega^2)\mathbb{G}^\alpha_{\pm a,\omega}(\boldsymbol{x},\boldsymbol{y}) = \mathcal{H}^\alpha\left[-\delta_{\boldsymbol{y}}\mathbb{I}\right], \quad \alpha = p, s. \tag{3.14}$$

Let us also introduce the decomposition of the operator $\mathcal{L}_{\lambda,\mu}$ into shear and pressure components as

$$\mathcal{L}_{\lambda,\mu} = \mathcal{L}^s_{\lambda,\mu} + \mathcal{L}^p_{\lambda,\mu}, \quad \text{and} \quad \mathcal{L}_{\eta_\lambda,\eta_\mu} = \mathcal{L}^s_{\eta_\lambda,\eta_\mu} + \mathcal{L}^p_{\eta_\lambda,\eta_\mu}, \tag{3.15}$$

where

$$\mathcal{L}^s_{\lambda,\mu}\mathbf{u} = c_s^2\left[\Delta\mathbf{u} - \nabla(\nabla\cdot\mathbf{u})\right] \quad \text{and} \quad \mathcal{L}^p_{\lambda,\mu}\mathbf{u} = c_p^2\nabla(\nabla\cdot\mathbf{u}), \tag{3.16}$$

and

$$\mathcal{L}^s_{\eta_\lambda,\eta_\mu}\mathbf{u} = \nu_s^2\left[\Delta\mathbf{u} - \nabla(\nabla\cdot\mathbf{u})\right] \quad \text{and} \quad \mathcal{L}^p_{\eta_\lambda,\eta_\mu}\mathbf{u} = \nu_p^2\nabla(\nabla\cdot\mathbf{u}). \tag{3.17}$$

Here, $\nu_s^2 = \eta_\mu$ and $\nu_p^2 = \eta_\lambda + 2\eta_\mu$. Therefore, the tensors $\mathbb{G}^s_{\pm a,\omega}$ and $\mathbb{G}^p_{\pm a,\omega}$ can also be seen as the solutions of

$$(\mathcal{L}^\alpha_{\lambda,\mu} \mp i\omega\mathcal{L}^\alpha_{\eta_\lambda,\eta_\mu} + \omega^2)\mathbb{G}^\alpha_{\pm a,\omega}(\boldsymbol{x},\boldsymbol{y}) = \mathcal{H}^\alpha\big[-\delta_{\boldsymbol{y}}\mathbb{I}\big](\boldsymbol{x}), \quad \alpha = p, s. \tag{3.18}$$

The corrected regularized time-reversal imaging functional defined by

$$\widetilde{\mathcal{I}}_{a,\rho} = c_s\mathcal{H}^s\left[\mathcal{I}_{a,\rho}\right] + c_p\mathcal{H}^p\left[\mathcal{I}_{a,\rho}\right], \tag{3.19}$$

is then given by

$$\widetilde{\mathcal{I}}_{a,\rho}(\boldsymbol{x}) = \int_{\partial\Omega}\int_0^T \frac{\partial}{\partial t}\left[c_p\mathbb{G}^p_{-a,\rho}(\boldsymbol{x},\boldsymbol{y},T-s) + c_s\mathbb{G}^s_{-a,\rho}(\boldsymbol{x},\boldsymbol{y},T-s)\right]\mathbf{g}_a(\boldsymbol{y},T-s)ds\,d\sigma(\boldsymbol{y}), \tag{3.20}$$

where

$$\mathbb{G}^\alpha_{-a,\rho}(\boldsymbol{x},\boldsymbol{y},t) = \frac{1}{2\pi}\int_{|\omega|\leq\rho}\mathbb{G}^\alpha_{-a,\omega}(\boldsymbol{x},\boldsymbol{y})\exp\left(-i\omega t\right)d\omega, \quad \alpha = p, s. \tag{3.21}$$

In the next subsection we express the relationship between the data $\mathbf{g}_a$ and the ideal measurements $\mathbf{g}$ obtained in the non-attenuated case. Doing so, we prove with the help of a new version of the Helmholtz-Kirchhoff identity that a regularized image of the source $\mathbf{F}$ can be obtained.

3.2 Attenuation operator and its asymptotics

Recall that $\mathbf{u}$ and $\mathbf{u}_a$ are respectively the solutions of the wave equations

$$\frac{\partial^2 \mathbf{u}}{\partial t^2}(\boldsymbol{x},t) - \mathcal{L}_{\lambda,\mu}\mathbf{u}(\boldsymbol{x},t) = \frac{d\delta_0(t)}{dt}\mathbf{F}(\boldsymbol{x}), \tag{3.22}$$

and

$$\frac{\partial^2 \mathbf{u}_a}{\partial t^2}(\boldsymbol{x},t) - \mathcal{L}_{\lambda,\mu}\mathbf{u}_a(\boldsymbol{x},t) - \frac{\partial}{\partial t}\mathcal{L}_{\eta_\lambda,\eta_\mu}\mathbf{u}_a(\boldsymbol{x},t) = \frac{d\delta_0(t)}{dt}\mathbf{F}(\boldsymbol{x}), \tag{3.23}$$

with the initial conditions

$$\mathbf{u}(\boldsymbol{x},t) = \mathbf{u}_a(\boldsymbol{x},t) = \frac{\partial \mathbf{u}}{\partial t}(\boldsymbol{x},t) = \frac{\partial \mathbf{u}_a}{\partial t}(\boldsymbol{x},t) = \mathbf{0}, \quad t<0. \tag{3.24}$$

We decompose $\mathbf{u}$ and $\mathbf{u}_a$ as

$$\mathbf{u} = \mathbf{u}^s + \mathbf{u}^p = \mathcal{H}^s[\mathbf{u}] + \mathcal{H}^p[\mathbf{u}] \quad \text{and} \quad \mathbf{u}_a = \mathbf{u}_a^s + \mathbf{u}_a^p = \mathcal{H}^s[\mathbf{u}_a] + \mathcal{H}^p[\mathbf{u}_a]. \tag{3.25}$$

The Fourier transforms $\mathbf{u}_\omega^\alpha$ and $\mathbf{u}_{a,\omega}^\alpha$ of the vector functions $\mathbf{u}^\alpha$ and $\mathbf{u}_a^\alpha$ are respectively solutions of

$$\left(\omega^2 + \mathcal{L}_{\lambda,\mu}^\alpha\right)\mathbf{u}_\omega^\alpha = i\omega\mathcal{H}^\alpha\left[\mathbf{F}\right] \quad \text{and} \quad \left(\kappa^\alpha(\omega)^2 + \mathcal{L}_{\lambda,\mu}^\alpha\right)\mathbf{u}_\omega^\alpha = i\frac{\kappa^\alpha(\omega)^2}{\omega}\mathcal{H}^\alpha\left[\mathbf{F}\right], \quad \alpha = p,s, \tag{3.26}$$

where

$$\kappa^\alpha(\omega) = \frac{\omega}{\sqrt{1-i\omega\nu_\alpha^2/c_\alpha^2}}. \tag{3.27}$$

In particular, it implies that

$$\mathbf{u}_a^s = \mathcal{A}_{\nu_s^2/c_s^2}\left[\mathbf{u}^s\right] \quad \text{and} \quad \mathbf{u}_a^p = \mathcal{A}_{\nu_p^2/c_p^2}\left[\mathbf{u}^p\right], \tag{3.28}$$

where $\mathcal{A}_a$, for $a>0$, is the attenuation operator

$$\mathcal{A}_a\left[\phi\right](t) = \frac{1}{2\pi}\int_{\mathbb{R}} \frac{\kappa_a(\omega)}{\omega}\left\{\int_{\mathbb{R}} \phi(s)\exp\{i\kappa_a(\omega)s\}ds\right\}\exp\{-i\omega t\}d\omega, \tag{3.29}$$

with $\kappa_a(\omega) = \dfrac{\omega}{\sqrt{1-i\omega a}}$.

We also define the operator $\mathcal{A}_{-a,\rho}$ by

$$\mathcal{A}_{-a,\rho}\left[\phi\right](t) = \frac{1}{2\pi}\int_{\mathbb{R}^+} \phi(s)\left\{\int_{|\omega|\le\rho} \frac{\kappa_{-a}(\omega)}{\omega}\exp\{i\kappa_{-a}(\omega)s\}\exp\{-i\omega t\}d\omega\right\}ds, \tag{3.30}$$

which is associated with $\kappa_{-a}(\omega) = \dfrac{\omega}{\sqrt{1+i\omega a}}$. Moreover, its adjoint operator $\mathcal{A}_{-a,\rho}^*$ reads

$$\mathcal{A}_{-a,\rho}^*\left[\phi\right](t) = \frac{1}{2\pi}\int_{|\omega|\le\rho} \frac{\kappa_{-a}(\omega)}{\omega}\exp\{i\kappa_{-a}(\omega)t\}\left\{\int_{\mathbb{R}^+} \phi(s)\exp\{-i\omega s\}ds\right\}d\omega. \tag{3.31}$$

Then, we have following results from [4, 5].

Proposition 3.2.

- *Let $\phi(t) \in \mathcal{S}([0,\infty))$, $\mathcal{S}$ being the Schwartz space. Then*

$$\mathcal{A}_a[\phi](t) = \phi(t) + \frac{a}{2}(t\phi')'(t) + o(a) \quad as \quad a \to 0. \tag{3.32}$$

- *Let $\phi(t) \in \mathcal{D}([0,\infty))$, where $\mathcal{D}([0,\infty))$ is the space of $\mathcal{C}^\infty$-functions of compact support on $[0,\infty)$. Then, for all ρ,*

$$\mathcal{A}^*_{-a,\rho}[\phi](t) = S_\rho[\phi](t) - \frac{a}{2} S_\rho\left[(t\phi')'\right](t) + o(a) \quad as \quad a \to 0. \tag{3.33}$$

- *Let $\phi(t) \in \mathcal{D}([0,\infty))$. Then, for all ρ,*

$$\mathcal{A}^*_{-a,\rho}\mathcal{A}_a[\phi](t) = S_\rho[\phi](t) + o(a) \quad as \quad a \to 0. \tag{3.34}$$

We extend the operators $\mathcal{A}_a$, $\mathcal{A}_{-a,\rho}$ and $\mathcal{A}^*_{-a,\rho}$ to tensors $\mathbb{G}$, *i.e.*, for all vectors $\boldsymbol{p} \in \mathbb{R}^d$,

$$\mathcal{A}_a[\mathbb{G}\boldsymbol{p}] = \mathcal{A}_a[\mathbb{G}]\boldsymbol{p}, \quad \mathcal{A}_{-a,\rho}[\mathbb{G}\boldsymbol{p}] = \mathcal{A}_{-a,\rho}[\mathbb{G}]\boldsymbol{p}, \quad \text{and} \quad \mathcal{A}^*_{-a,\rho}[\mathbb{G}\boldsymbol{p}] = \mathcal{A}^*_{-a,\rho}[\mathbb{G}]\boldsymbol{p}.$$

By the definition of the operators $\mathcal{A}_a$ and $\mathcal{A}_{-a,\rho}$, we have for $\alpha = p, s$:

$$\frac{\partial \mathbb{G}^\alpha_a}{\partial t}(\boldsymbol{x},\boldsymbol{y},t) = \mathcal{A}_{\nu^2_\alpha/c^2_\alpha}\left[\frac{\partial \mathbb{G}^\alpha}{\partial t}(\boldsymbol{x},\boldsymbol{y},\cdot)\right](t), \tag{3.35}$$

$$\frac{\partial \mathbb{G}^\alpha_{-a,\rho}}{\partial t}(\boldsymbol{x},\boldsymbol{y},t) = \mathcal{A}_{-\nu^2_\alpha/c^2_\alpha,\rho}\left[\frac{\partial \mathbb{G}^\alpha}{\partial t}(\boldsymbol{x},\boldsymbol{y},\cdot)\right](t). \tag{3.36}$$

Recall that $\mathbf{g} = \mathbf{u}$ and $\mathbf{g}_a = \mathbf{u}_a$ on $\partial\Omega \times \mathbb{R}$. It then follows from (3.28) that, for $\alpha = p, s$,

$$\mathcal{A}^*_{-\nu^2_\alpha/c^2_\alpha,\rho}\mathcal{A}_{\nu^2_\alpha/c^2_\alpha}[\mathbf{g}^\alpha_a] = S_\rho[\mathbf{g}^\alpha] + o(a), \tag{3.37}$$

where

$$\mathbf{g}^\alpha_a = \mathcal{H}^\alpha[\mathbf{g}_a], \quad \mathbf{g}^\alpha = \mathcal{H}^\alpha[\mathbf{g}]. \tag{3.38}$$

Identity (3.37) proves that $\mathcal{A}^*_{-\nu^2_\alpha/c^2_\alpha,\rho}$ is an approximate inverse of $\mathcal{A}_{\nu^2_\alpha/c^2_\alpha}$. Moreover, it plays a key role in showing that the regularized time reversal algorithm provides a first-order correction of the attenuation effect.

3.3 Helmholtz-Kirchhoff identity in an attenuating media

In this subsection we derive a new Helmholtz-Kirchhoff identity in elastic attenuating media. For doing so, let us introduce the conormal derivatives $\frac{\partial \mathbf{u}}{\partial \nu_a}$ and $\frac{\partial \mathbf{u}}{\partial \nu_{-a}}$ as follows:

$$\frac{\partial \mathbf{u}}{\partial \nu_{\pm a}} := \left(\lambda(\nabla\cdot\mathbf{u})\boldsymbol{n} + \mu(\nabla\mathbf{u}^T + (\nabla\mathbf{u}^T)^T)\boldsymbol{n}\right) \mp i\omega\left(\eta_\lambda(\nabla\cdot\mathbf{u})\boldsymbol{n} + \eta_\mu(\nabla\mathbf{u}^T + (\nabla\mathbf{u}^T)^T)\boldsymbol{n}\right). \tag{3.39}$$

Note also that for a tensor $\mathbb{G}$ the conormal derivative $\frac{\partial \mathbb{G}}{\partial \nu_{\pm a}}$ means that for all constant vectors $\boldsymbol{p}$,

$$\left[\frac{\partial \mathbb{G}}{\partial \nu_{\pm a}}\right]\boldsymbol{p} := \frac{\partial[\mathbb{G}\boldsymbol{p}]}{\partial \nu_{\pm a}}. \tag{3.40}$$

The following properties hold.

Proposition 3.3. *For all $\boldsymbol{x}, \boldsymbol{z} \in \Omega$, we have*

$$\int_{\partial\Omega} \left[\frac{\partial \mathbb{G}^s_{-a,\omega}(\boldsymbol{x},\boldsymbol{y})}{\partial \nu_{-a}} \overline{\mathbb{G}^p_{a,\omega}}(\boldsymbol{y},\boldsymbol{z}) - \mathbb{G}^s_{-a,\omega}(\boldsymbol{x},\boldsymbol{y}) \overline{\frac{\partial \mathbb{G}^p_{a,\omega}(\boldsymbol{y},\boldsymbol{z})}{\partial \nu_a}} \right] d\sigma(\boldsymbol{y}) = 0. \tag{3.41}$$

Proof. Note that

$$\begin{aligned}
\mathcal{J} &:= \int_{\partial\Omega} \left[\frac{\partial \mathbb{G}^s_{-a,\omega}(\boldsymbol{x},\boldsymbol{y})}{\partial \nu_{-a}} \overline{\mathbb{G}^p_{a,\omega}}(\boldsymbol{y},\boldsymbol{z}) - \mathbb{G}^s_{-a,\omega}(\boldsymbol{x},\boldsymbol{y}) \overline{\frac{\partial \mathbb{G}^p_{a,\omega}(\boldsymbol{y},\boldsymbol{z})}{\partial \nu_a}} \right] d\sigma(\boldsymbol{y}) \\
&= \int_{\partial\Omega} \left[\frac{\partial \mathbb{G}^s_{-a,\omega}(\boldsymbol{x},\boldsymbol{y})}{\partial \nu_{-a}} \overline{\mathbb{G}^p_{a,\omega}}(\boldsymbol{y},\boldsymbol{z}) - \mathbb{G}^s_{-a,\omega}(\boldsymbol{x},\boldsymbol{y}) \frac{\partial \overline{\mathbb{G}^p_{a,\omega}}(\boldsymbol{y},\boldsymbol{z})}{\partial \nu_{-a}} \right] d\sigma(\boldsymbol{y}) \\
&= \int_{\Omega} \left[\mathcal{L}_{\lambda,\mu} \mathbb{G}^s_{-a,\omega}(\boldsymbol{x},\boldsymbol{y}) + i\omega \mathcal{L}_{\eta_\lambda,\eta_\mu} \mathbb{G}^s_{-a,\omega}(\boldsymbol{x},\boldsymbol{y}) \right] \overline{\mathbb{G}^p_{a,\omega}}(\boldsymbol{y},\boldsymbol{z})\, d\boldsymbol{y} \\
&\qquad - \int_{\Omega} \mathbb{G}^s_{-a,\omega}(\boldsymbol{x},\boldsymbol{y}) \left[\mathcal{L}_{\lambda,\mu} \overline{\mathbb{G}^p_{a,\omega}}(\boldsymbol{y},\boldsymbol{z}) + i\omega \mathcal{L}_{\eta_\lambda,\eta_\mu} \overline{\mathbb{G}^p_{a,\omega}}(\boldsymbol{y},\boldsymbol{z}) \right] d\boldsymbol{y}, \\
&= \int_{\Omega} \left[\mathcal{L}_{\lambda,\mu} \mathbb{G}^s_{-a,\omega}(\boldsymbol{x},\boldsymbol{y}) + i\omega \mathcal{L}_{\eta_\lambda,\eta_\mu} \mathbb{G}^s_{-a,\omega}(\boldsymbol{x},\boldsymbol{y}) \right] \overline{\mathbb{G}^p_{a,\omega}}(\boldsymbol{y},\boldsymbol{z})\, d\boldsymbol{y} \\
&\qquad - \int_{\Omega} \mathbb{G}^s_{-a,\omega}(\boldsymbol{x},\boldsymbol{y}) \overline{\left[\mathcal{L}_{\lambda,\mu} \mathbb{G}^p_{a,\omega}(\boldsymbol{y},\boldsymbol{z}) - i\omega \mathcal{L}_{\eta_\lambda,\eta_\mu} \mathbb{G}^p_{a,\omega}(\boldsymbol{y},\boldsymbol{z}) \right]}\, d\boldsymbol{y}.
\end{aligned}$$

Since $\mathbb{G}^p_{a,\omega}(\boldsymbol{x},\boldsymbol{y})$ and $\mathbb{G}^s_{-a,\omega}(\boldsymbol{x},\boldsymbol{y})$ are solutions of equations (3.14) with $\alpha = p, s$, respectively, it follows that

$$\mathcal{J} = [\mathcal{H}^s[-\delta_{\mathbf{0}}\mathbb{I}] * \overline{\mathbb{G}^p_{a,\omega}}(\cdot,\boldsymbol{z})](\boldsymbol{x}) - [\mathbb{G}^s_{-a,\omega}(\boldsymbol{x},\cdot) * \mathcal{H}^p[-\delta_{\mathbf{0}}\mathbb{I}]](\boldsymbol{z}).$$

As in the proof of Proposition 2.2 one can show that

$$[\mathcal{H}^s[-\delta_{\mathbf{0}}\mathbb{I}] * \overline{\mathbb{G}^p_{a,\omega}}(\cdot,\boldsymbol{z})](\boldsymbol{x}) = 0 \quad \text{and} \quad [\mathbb{G}^s_{-a,\omega}(\boldsymbol{x},\cdot) * \mathcal{H}^p[-\delta_{\mathbf{0}}\mathbb{I}]](\boldsymbol{z}) = 0,$$

which completes the proof of the proposition. □

We now give an approximation of the attenuating co-normal derivative.

Proposition 3.4. *If $\boldsymbol{n} = \widehat{\boldsymbol{y}-\boldsymbol{x}}$, then for $\alpha = p, s$, we have*

$$\frac{\partial \mathbb{G}^\alpha_{\pm a,\omega}(\boldsymbol{x},\boldsymbol{y})}{\partial \nu_{\pm a}} \simeq \frac{i c_\alpha \omega^2}{\kappa^\alpha_\mp(\omega)} \mathbb{G}^\alpha_{\pm a,\omega}(\boldsymbol{x},\boldsymbol{y}), \tag{3.42}$$

where

$$\kappa^\alpha_\mp(\omega) = \frac{\omega}{\sqrt{1 \mp i\omega\nu_\alpha^2/c_\alpha^2}}. \tag{3.43}$$

Proof. Indeed, notice that

$$\mathbb{G}^\alpha_{\pm a,\omega}(\boldsymbol{x},\boldsymbol{y}) = \left[\frac{\kappa^\alpha_\mp(\omega)}{\omega} \right]^2 \mathbb{G}^\alpha_{\kappa^\alpha_\mp(\omega)}(\boldsymbol{x},\boldsymbol{y}), \quad \alpha = p, s. \tag{3.44}$$

Then, from Proposition 2.4, we obtain

$$\begin{aligned}\frac{\partial \mathbb{G}^{\alpha}_{\pm a,\omega}(\boldsymbol{x},\boldsymbol{y})}{\partial \nu_{\pm a}} &\simeq \left[\frac{\kappa^{\alpha}_{\mp}(\omega)}{\omega}\right]^2 \left(\left(ic_{\alpha}^2\frac{\kappa^{\alpha}_{\mp}(\omega)}{c_{\alpha}}\mathbb{G}^{\alpha}_{\kappa^{\alpha}_{\mp}(\omega)}(\boldsymbol{x},\boldsymbol{y})\right) \mp i\omega\left(i\nu_{\alpha}^2\frac{\kappa^{\alpha}_{\mp}(\omega)}{c_{\alpha}}\mathbb{G}^{\alpha}_{\kappa^{\alpha}_{\mp}(\omega)}(\boldsymbol{x},\boldsymbol{y})\right)\right) \\ &\simeq \left[ic_{\alpha}\kappa^{\alpha}_{\mp}(\omega)\left(1 \mp i\omega\nu_{\alpha}^2/c_{\alpha}^2\right)\right]\mathbb{G}^{\alpha}_{\pm a,\omega}(\boldsymbol{x},\boldsymbol{y}) \simeq \frac{ic_{\alpha}\omega^2}{\kappa^{\alpha}_{\mp}(\omega)}\mathbb{G}^{\alpha}_{\pm a,\omega}(\boldsymbol{x},\boldsymbol{y}).\end{aligned}$$

□

In particular, the following estimate holds as a direct consequence of Propositions 3.3 and 3.4.

Proposition 3.5. *Let $\Omega \subset \mathbb{R}^d$ be a ball with radius R. Then for all $\boldsymbol{x}, \boldsymbol{z} \in \Omega$ sufficiently far from boundary $\partial\Omega$, we have*

$$\Re e\left\{\int_{\partial\Omega}\mathbb{G}^{s}_{-a,\omega}(\boldsymbol{x},\boldsymbol{y})\overline{\mathbb{G}^{p}_{a,\omega}}(\boldsymbol{y},\boldsymbol{z})d\sigma(\boldsymbol{y})\right\} \simeq \Re e\left\{\int_{\partial\Omega}\mathbb{G}^{p}_{-a,\omega}(\boldsymbol{x},\boldsymbol{y})\overline{\mathbb{G}^{s}_{a,\omega}}(\boldsymbol{y},\boldsymbol{z})d\sigma(\boldsymbol{y})\right\} \simeq 0. \tag{3.45}$$

3.4 Analysis of the regularized time-reversal imaging algorithm

The aim of this subsection is to justify that the regularized time-reversal imaging functional $\widetilde{\mathcal{I}}_{a,\rho}$ provides a correction of the attenuation effect.

Theorem 3.6. *The regularized time-reversal imaging functional $\widetilde{\mathcal{I}}_{a,\rho}$ satisfies*

$$\widetilde{\mathcal{I}}_{a,\rho}(\boldsymbol{x}) = \widetilde{\mathcal{I}}_{\rho}(\boldsymbol{x}) + o\left(\nu_s^2/c_s^2 + \nu_p^2/c_p^2\right), \tag{3.46}$$

$$\widetilde{\mathcal{I}}_{\rho}(\boldsymbol{x}) := \int_{\partial\Omega}\int_0^T \left[c_s\frac{\partial}{\partial t}\mathbb{G}^{s}(\boldsymbol{x},\boldsymbol{y},s) + c_p\frac{\partial}{\partial t}\mathbb{G}^{p}(\boldsymbol{x},\boldsymbol{y},s)\right] S_{\rho}\left[\mathbf{g}(\boldsymbol{y},\cdot)\right](s)ds\, d\sigma(\boldsymbol{y}), \tag{3.47}$$

where S_ρ is defined by (3.11).

Proof. We can decompose the functional $\widetilde{\mathcal{I}}_{a,\rho}$ as follows:

$$\begin{aligned}\widetilde{\mathcal{I}}_{a,\rho}(\boldsymbol{x}) &= \int_{\partial\Omega}\int_0^T \frac{\partial}{\partial t}\left[c_p\mathbb{G}^{p}_{-a,\rho}(\boldsymbol{x},\boldsymbol{y},T-s) + c_s\mathbb{G}^{s}_{-a,\rho}(\boldsymbol{x},\boldsymbol{y},T-s)\right]\mathbf{g}_a(\boldsymbol{y},T-s)ds\, d\sigma(\boldsymbol{y}) \\ &= \int_{\partial\Omega}\int_0^T \frac{\partial}{\partial t}\left[c_p\mathbb{G}^{p}_{-a,\rho}(\boldsymbol{x},\boldsymbol{y},s) + c_s\mathbb{G}^{s}_{-a,\rho}(\boldsymbol{x},\boldsymbol{y},s)\right]\left[\mathbf{g}^{s}_a(\boldsymbol{y},s) + \mathbf{g}^{p}_a(\boldsymbol{y},s)\right]ds\, d\sigma(\boldsymbol{y}) \\ &= \mathcal{I}^{ss}_{a,\rho}(\boldsymbol{x}) + \mathcal{I}^{sp}_{a,\rho}(\boldsymbol{x}) + \mathcal{I}^{ps}_{a,\rho}(\boldsymbol{x}) + \mathcal{I}^{pp}_{a,\rho}(\boldsymbol{x}),\end{aligned}$$

where

$$\mathcal{I}^{\alpha\beta}_{a,\rho}(\boldsymbol{x}) = \int_{\partial\Omega}\int_0^T \frac{\partial}{\partial t}\left[c_{\alpha}\mathbb{G}^{\alpha}_{-a,\rho}(\boldsymbol{x},\boldsymbol{y},s)\right]\mathbf{g}^{\beta}_a(\boldsymbol{y},s)ds\, d\sigma(\boldsymbol{y}), \quad \alpha,\beta \in \{p,s\}.$$

Similarly we can decompose the functional $\widetilde{\mathcal{I}}_{\rho}$ as

$$\widetilde{\mathcal{I}}_{\rho}(\boldsymbol{x}) = \mathcal{I}^{ss}_{\rho}(\boldsymbol{x}) + \mathcal{I}^{sp}_{\rho}(\boldsymbol{x}) + \mathcal{I}^{ps}_{\rho}(\boldsymbol{x}) + \mathcal{I}^{pp}_{\rho}(\boldsymbol{x}),$$

with

$$\mathcal{I}_\rho^{\alpha\beta}(\boldsymbol{x}) = \int_{\partial\Omega}\int_0^T \frac{\partial}{\partial t}\left[c_\alpha \mathbb{G}^\alpha(\boldsymbol{x},\boldsymbol{y},s)\right] S_\rho[\mathbf{g}^\beta(\boldsymbol{y},\cdot)](s)ds\, d\sigma(\boldsymbol{y}), \quad \alpha,\beta\in\{p,s\}.$$

The first term $\mathcal{I}_{a,\rho}^{ss}(\boldsymbol{x})$ satisfies

$$\begin{aligned}
\mathcal{I}_{a,\rho}^{ss}(\boldsymbol{x}) &= \int_{\partial\Omega}\int_0^T \mathcal{A}_{-\nu_s^2/c_s^2,\rho}\left[\frac{\partial}{\partial t}\left[c_s\mathbb{G}^s(\boldsymbol{x},\boldsymbol{y},s)\right]\right]\mathcal{A}_{\nu_s^2/c_s^2}\left[\mathbf{g}^s(\boldsymbol{y},\cdot)\right](s)ds\, d\sigma(\boldsymbol{y})\\
&= \int_{\partial\Omega}\int_0^T \frac{\partial}{\partial t}\left[c_s\mathbb{G}^s(\boldsymbol{x},\boldsymbol{y},s)\right]\mathcal{A}^*_{-\nu_s^2/c_s^2,\rho}\left[\mathcal{A}_{\nu_s^2/c_s^2}\left[\mathbf{g}^s(\boldsymbol{y},\cdot)\right]\right](s)ds\, d\sigma(\boldsymbol{y})\\
&= \int_{\partial\Omega}\int_0^T \frac{\partial}{\partial t}\left[c_s\mathbb{G}^s(\boldsymbol{x},\boldsymbol{y},s)\right] S_\rho\left[\mathbf{g}^s(\boldsymbol{y},\cdot)\right](s)ds\, d\sigma(\boldsymbol{y}) + o\left(\nu_s^2/c_s^2\right)\\
&= \mathcal{I}_\rho^{ss}(\boldsymbol{x}) + o\left(\nu_s^2/c_s^2\right),
\end{aligned}$$

by using Proposition 3.2. Similarly, we get

$$\mathcal{I}_{a,\rho}^{pp}(\boldsymbol{x}) = \mathcal{I}_\rho^{pp}(\boldsymbol{x}) + o\left(\nu_p^2/c_p^2\right).$$

Moreover, the coupling terms $\mathcal{I}_{a,\rho}^{sp}$ and $\mathcal{I}_{a,\rho}^{ps}$ vanish. Indeed, thanks to Proposition 3.5, we have

$$\mathcal{I}_{a,\rho}^{sp}(\boldsymbol{x}) = \frac{1}{2\pi}\int_{\mathbb{R}^d}\int_{|\omega|<\rho}\omega^2\left[\int_{\partial\Omega}\left[c_s\mathbb{G}^s_{-a,\omega}(\boldsymbol{x},\boldsymbol{y})\right]\overline{\mathbb{G}^p_{a,\omega}}(\boldsymbol{y},\boldsymbol{z})\, d\sigma(\boldsymbol{y})\right] d\omega\mathbf{F}(\boldsymbol{z})\, d\boldsymbol{z} \simeq 0,$$

and

$$\mathcal{I}_{a,\rho}^{ps}(\boldsymbol{x}) = \frac{1}{2\pi}\int_{\mathbb{R}^d}\int_{|\omega|<\rho}\omega^2\left[\int_{\partial\Omega}\left[c_p\mathbb{G}^p_{-a,\omega}(\boldsymbol{x},\boldsymbol{y})\right]\overline{\mathbb{G}^s_{a,\omega}}(\boldsymbol{y},\boldsymbol{z})\, d\sigma(\boldsymbol{y})\right] d\omega\mathbf{F}(\boldsymbol{z})\, d\boldsymbol{z} \simeq 0.$$

Proposition 2.5 shows that we also have

$$\begin{aligned}
\mathcal{I}_\rho^{sp}(\boldsymbol{x}) &= \frac{1}{2\pi}\int_{\mathbb{R}^d}\int_{|\omega|<\rho}\omega^2\left[\int_{\partial\Omega}\left[c_s\mathbb{G}^s_{\omega}(\boldsymbol{x},\boldsymbol{y})\right]\overline{\mathbb{G}^p_{\omega}}(\boldsymbol{y},\boldsymbol{z})\, d\sigma(\boldsymbol{y})\right] d\omega\mathbf{F}(\boldsymbol{z})\, d\boldsymbol{z} \simeq 0,\\
\mathcal{I}_\rho^{ps}(\boldsymbol{x}) &= \frac{1}{2\pi}\int_{\mathbb{R}^d}\int_{|\omega|<\rho}\omega^2\left[\int_{\partial\Omega}\left[c_p\mathbb{G}^p_{\omega}(\boldsymbol{x},\boldsymbol{y})\right]\overline{\mathbb{G}^s_{\omega}}(\boldsymbol{y},\boldsymbol{z})\, d\sigma(\boldsymbol{y})\right] d\omega\mathbf{F}(\boldsymbol{z})\, d\boldsymbol{z} \simeq 0,
\end{aligned}$$

which concludes the proof. □

It is straightforward to check that

$$\widetilde{\mathcal{I}}_\rho(\boldsymbol{x}) \overset{\rho\to\infty}{\longrightarrow} \widetilde{\mathcal{I}}(\boldsymbol{x}) \simeq \mathbf{F}(\boldsymbol{x}), \tag{3.48}$$

by Theorem 2.6. Therefore, $\widetilde{\mathcal{I}}_{a,\rho}$ provides a first-order correction in terms of $\nu_s^2/c_s^2 + \nu_p^2/c_p^2$ of the attenuation effect. Moreover, the imaging functional $\widetilde{\mathcal{I}}_{a,\rho}$ can be seen as the time-reversal functional $\widetilde{\mathcal{I}}$ defined by (2.7) applied to $\mathcal{A}^*_{-\nu_\alpha^2/c_\alpha^2,\rho}\mathbf{g}_a^\alpha, \alpha = p,s$. As shown in (3.34), the regularized operators $\mathcal{A}^*_{-a,\rho}$ give a first-order approximation of the inverse of $\mathcal{A}_a$ for $a = \nu_\alpha^2/c_\alpha^2$. It would be very interesting to construct higher-order reconstructions in terms of the attenuation effect using higher-order approximations of the inverse of the operator

$\mathcal{A}_a$. The problem is more challenging than the one in the scalar case [4] because of the coupling between the shear and pressure components. Note finally that, if one applies the time-reversal functional $\widetilde{\mathcal{I}}$ to the data $\mathbf{g}_a$ directly, then one finds

$$\begin{aligned}\widetilde{\mathcal{I}}(\boldsymbol{x}) &= \int_{\partial\Omega}\int_0^T \frac{\partial}{\partial t}\left[c_p\mathbb{G}^p(\boldsymbol{x},\boldsymbol{y},s)+c_s\mathbb{G}^s(\boldsymbol{x},\boldsymbol{y},s)\right]\left[\mathbf{g}_a(\boldsymbol{y},\cdot)\right](s)\,ds\,d\sigma(\boldsymbol{y}) \\ &= \frac{1}{2\pi}\int_{\mathbb{R}^d}\int_{\mathbb{R}}\omega^2\left[\int_{\partial\Omega}\left[c_p\mathbb{G}^p_\omega(\boldsymbol{x},\boldsymbol{y})+c_s\mathbb{G}^s_\omega(\boldsymbol{x},\boldsymbol{y})\right]\overline{\mathbb{G}_{a,\omega}}(\boldsymbol{y},\boldsymbol{z})d\sigma(\boldsymbol{y})\right]d\omega\mathbf{F}(\boldsymbol{z})d\boldsymbol{z}, \quad (3.49)\end{aligned}$$

which gives an error of the order of $\nu_s^2/c_s^2+\nu_p^2/c_p^2$ as can be seen from the expansion (3.32).

3.5 Numerical simulations

In this section we present numerical illustrations and describe our algorithms for numerical resolution of the source problem to show that $\widetilde{\mathcal{I}}_{a,\rho}$ provides a better reconstruction than $\widetilde{\mathcal{I}}$, where the attenuation effect is not taken into account.

3.5.1 Description of the algorithm

In the expression of $\widetilde{\mathcal{I}}_{a,\rho}$, the solution $\mathbf{v}_{s,a,\rho}(\boldsymbol{x},t)$ is very difficult to obtain numerically. Therefore, we prefer to regularize the problem by truncating high-frequency components in space instead of time, in contrast with our theoretical analysis. This can be seen as an approximation $\tilde{\mathbf{v}}_{s,a,\rho}(\boldsymbol{x},t)$ of $\mathbf{v}_{s,a,\rho}(\boldsymbol{x},t)$ defined as the solution of

$$\frac{\partial^2\tilde{\mathbf{v}}_{s,a,\rho}}{\partial t^2}(\boldsymbol{x},t)-\mathcal{L}_{\lambda,\mu}\tilde{\mathbf{v}}_{s,a,\rho}(\boldsymbol{x},t)+\frac{\partial}{\partial t}\mathcal{L}_{\eta_\lambda,\eta_\mu}\tilde{\mathbf{v}}_{s,a,\rho}(\boldsymbol{x},t)=\frac{\partial\delta_s(t)}{\partial t}\mathcal{X}_\rho\left[\mathbf{g}_a(\cdot,T-s)\delta_{\partial\Omega}\right](\boldsymbol{x}),$$

where the operator $\mathcal{X}_\rho$ is defined by

$$\mathcal{X}_\rho\left[\mathbf{g}_a(\cdot,T-s)\delta_{\partial\Omega}\right](\boldsymbol{x})=\int_{|\boldsymbol{k}|\le\rho}\left[\int_{\partial\Omega}\mathbf{g}_a(\boldsymbol{y},T-s)e^{-2i\pi\boldsymbol{k}\cdot\boldsymbol{y}}\,d\sigma(\boldsymbol{y})\right]e^{2i\pi\boldsymbol{k}\cdot\boldsymbol{x}}d\boldsymbol{k}\;\delta_{\partial\Omega}(\boldsymbol{x}).$$

The operator $\mathcal{X}_\rho$, as the operator S_ρ, truncates high frequencies but in the space variable.

To compute the solution of the viscoelastic wave equation in two dimensions

$$\frac{\partial^2\mathbf{u}_a}{\partial t^2}(\boldsymbol{x},t)-\mathcal{L}_{\lambda,\mu}\mathbf{u}_a(\boldsymbol{x},t)\pm\mathcal{L}_{\eta_\lambda,\eta_\mu}\mathbf{u}_a(\boldsymbol{x},t)=\mathbf{0},$$

we use the same algorithm presented in the unattenuated case, *i.e.*, we use a larger box $\Omega\subset Q=[-L/2,L/2]^2$ with periodic boundary condition and again a *splitting spectral Fourier* approach coupled with a PML technique to simulate a free outgoing interface on ∂Q.

3.5.2 Experiments

In the sequel, for numerical illustrations, Ω is taken to be a unit disc. Its boundary is discretized by 2^{11} sensors. Each solution of elastic wave equation is computed over $(\boldsymbol{x},t)\in[-L/2,L/2]^2\times[0,T]$ with $L=4$ and $T=2$. We use a step of discretization

given by $dt = T/2^{13}$ and $dx = L/2^9$.

Figure 4 presents a first experiment with Lamé parameters $(\lambda, \mu) = (1, 1)$ and attenuation coefficients $(\eta_\lambda, \eta_\mu) = (0.0002, 0.0002)$. The first line corresponds to the two components of the initial source $\mathbf{F}$. The second line corresponds to the reconstruction of $\mathbf{F}$ without taking into account the attenuation effect. The imaging functional $\widetilde{\mathcal{I}}(\boldsymbol{x})$ appears to be blurred due to coupling effects. The three last lines correspond to a reconstruction of $\mathbf{F}$ using the imaging functional $\widetilde{\mathcal{I}}_{a,\rho}$ for different values of ρ. We clearly observe a better reconstruction of the source $\mathbf{F}$ than using the functional $\widetilde{\mathcal{I}}$ provided that the regularization parameter ρ is chosen appropriately large in order to insure the good resolution of the reconstruction.

Figures 5 and 6 present two other examples of reconstruction using $\widetilde{\mathcal{I}}_{a,\rho}$. The same observation holds.

References

[1] K. Aki and P. G. Richards, *Quantitative Seismology*, Vol. 1, W.H. Freeman and Co., San Francisco, 1980.

[2] H. Ammari, *An Introduction to Mathematics of Emerging Biomedical Imaging*, Mathematics & Applications, Vol. 62, Springer-Verlag, Berlin, 2008.

[3] H. Ammari, E. Bretin, J. Garnier, and A. Wahab, Noise Source Localization in an Attenuating Medium, SIAM J. Appl. Math., to appear.

[4] H. Ammari, E. Bretin, J. Garnier, and A. Wahab, Time reversal in attenuating acoustic media, *Mathematical and Statistical Methods for Imaging*, Contemporary Mathematics, Vol. 548, 151–163, Amer. Math. Soc., Providence, RI, 2011.

[5] H. Ammari, E. Bretin, V. Jugnon, and A. Wahab, Photoacoustic imaging for attenuating acoustic media, in *Mathematical Modeling in Biomedical Imaging II*, Lecture Notes in Mathematics, Vol. 2035, 53–80, Springer-Verlag, Berlin, 2011.

[6] H. Ammari, E. Bossy, V. Jugnon, and H. Kang, Mathematical modelling in photoacoustic imaging of small absorbers, SIAM Review, 52 (2010), 677–695.

[7] H. Ammari, Y. Capdeboscq, H. Kang, and A. Kozhemyak, Mathematical models and reconstruction methods in magneto-acoustic imaging, Euro. J. Appl. Math., 20 (2009), 303–317.

[8] H. Ammari, P. Garapon, L. Guadarrama Bustos, and H. Kang, Transient anomaly imaging by the acoustic radiation force, J. Diff. Equat., 249 (2010), 1579–1595.

[9] H. Ammari, P. Garapon, H. Kang, and H. Lee, A method of biological tissues elasticity reconstruction using magnetic resonance elastography measurements, Quart. Appl. Math., 66 (2008), 139–175.

[10] H. Ammari, L. Guadarrama-Bustos, H. Kang, and H. Lee, Transient elasticity imaging and time reversal, Proceedings of the Royal Society of Edinburgh: Section A Mathematics, to appear.

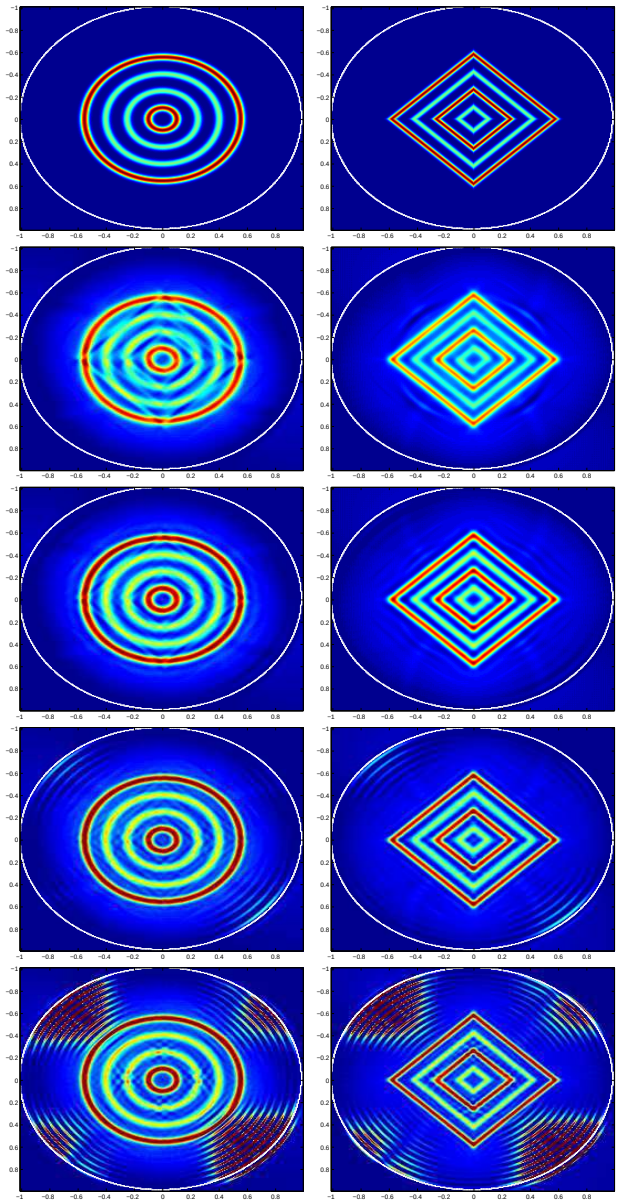

Figure 4: Test 4: Comparison between $\widetilde{\mathcal{I}}$ and $\widetilde{\mathcal{I}}_{a,\rho}$ in a viscoelastic medium; The parameters are $(\lambda, \mu) = (1, 1)$ and $(\nu_s^2/c_s^2, \nu_p^2/c_p^2) = (0.0002, 0.0002)$; First (top) line: initial condition; Second line: without correction of attenuation; Last lines: with $\widetilde{\mathcal{I}}_{a,\rho}$ and $\rho = 15, 20, 25$.

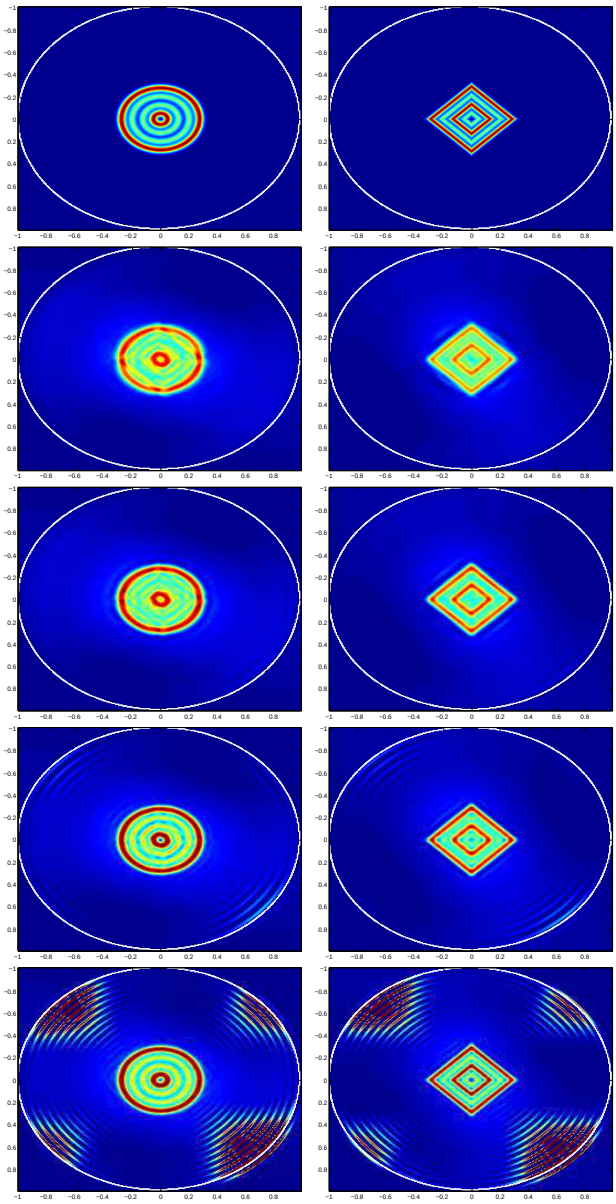

Figure 5: Test 5: Comparison between $\widetilde{\mathcal{I}}$ and $\widetilde{\mathcal{I}}_{a,\rho}$ in a viscoelastic medium; The parameters are $(\lambda, \mu) = (1, 1)$ and $(\nu_s^2/c_s^2, \nu_p^2/c_p^2) = (0.00005, 0.00005)$; First line: initial condition; Second line: without correction of attenuation; Last lines: with $\widetilde{\mathcal{I}}_{a,\rho}$ and $\rho = 15, 20, 25$.

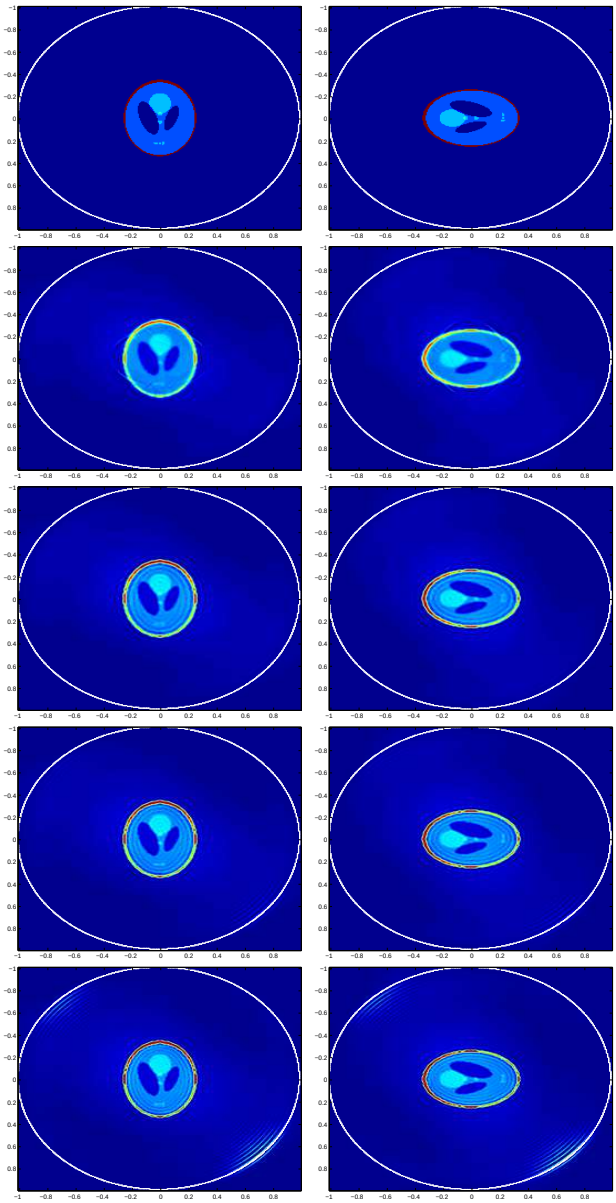

Figure 6: Test 6: Comparison between $\widetilde{\mathcal{I}}$ and $\widetilde{\mathcal{I}}_{a,\rho}$ in a viscoelastic medium; The parameters are $(\lambda, \mu) = (1, 1)$ and $(\eta_\lambda, \eta_\mu) = (0.00005, 0.00005)$; First line: initial source $\mathbf{F}$; Second line: reconstruction of $\mathbf{F}$ using $\widetilde{\mathcal{I}}$; Three last lines: reconstruction of $\mathbf{F}$ using $\widetilde{\mathcal{I}}_{a,\rho}$ with respectively $\rho = 25, 30, 35$.

[11] H. Ammari and H. Kang, *Polarization and Moment Tensors: with Applications to Inverse Problems and Effective Medium Theory*, Applied Mathematical Sciences Series, Vol. 162, Springer-Verlag, New York, 2007.

[12] J. Bercoff, M. Tanter, M. Muller, and M. Fink, The role of viscosity in the impulse diffraction field of elastic waves induced by the acoustic radiation force, IEEE Trans. Ultrasonics, Ferro., Freq. Control, 51 (2004), 1523–1536.

[13] L. Borcea, G. Papanicolaou, C. Tsogka, and J. G. Berrymann, Imaging and time reversal in random media, Inverse Problems, 18 (2002), 1247–1279.

[14] E. Bretin, L. Guadarrama Bustos, and A. Wahab, On the Green function in visco-elastic media obeying a frequency power-law, Math. Meth. Appl. Sci., 34 (2011), 819–830.

[15] C. Canuto, M. Y. Hussaini, A. Quarteroni, and T. A. Zang, *Spectral Methods in Fluid Dynamics*, Springer-Verlag, New York-Heidelberg-Berlin, 1987.

[16] S. Catheline, N. Benech, J. Brum, and C. Negreira, Time-reversal of elastic waves in soft solids, Phys. Rev. Lett., 100 (2008), 064301.

[17] J. de Rosny, G. Lerosey, A. Tourin, and M. Fink, Time reversal of electromagnetic waves, In *Lecture Notes in Comput. Sci. Eng.*, Vol. 59, 2007.

[18] M. Fink, Time reversed acoustics, Physics Today 50 (1997), 34.

[19] M. Fink and C. Prada, Acoustic time-reversal mirrors, Inverse Problems, 17 (2001), R1–R38.

[20] J.-P. Fouque, J. Garnier, G. Papanicolaou, and K. Sølna, *Wave Propagation and Time Reversal in Randomly Layered Media*, Springer, New York, 2007.

[21] J.F. Greenleaf, M. Fatemi, and M. Insana, Selected methods for imaging elastic properties of biological tissues, Annu. Rev. Biomed. Eng., 5 (2003), 57–78.

[22] F. Hastings, J.B. Schneider, and S. L. Broschat, Application of the perfectly matched layer (PML) absorbing boundary condition to elastic wave propagation, J. Acoust. Soc. Am., 100 (1996), 3061–3069.

[23] L. Hörmander, *The Analysis of Linear Partial Differential Operators. I. Distribution Theory and Fourier Analysis*, Classics in Mathematics, Springer-Verlag, Berlin, 2003.

[24] R. Kowar and O. Scherzer, Photoacoustic imaging taking into account attenuation, in *Mathematical Modeling in Biomedical Imaging II*, Lecture Notes in Mathematics, Vol. 2035, 85–130, Springer-Verlag, Berlin, 2011.

[25] R. Kowar, O. Scherzer, and X. Bonnefond, Causality analysis of frequency dependent wave attenuation, Math. Meth. Appl. Sci., 34 (2011), 108–124.

[26] C. Larmat, J.P. Montagner, M. Fink, Y. Capdeville, A. Tourin, and E. Clévédé, Time-reversal imaging of seismic sources and application to the great Sumatra earthquake, Geophys. Res. Lett., 33 (2006), L19312.

[27] G. Lerosey, J. de Rosny, A. Tourin, A. Derode, G. Montaldo, and M. Fink, Time-reversal of electromagnetic waves and telecommunication, Radio Sci. 40, (2005), RS6S12.

[28] P. D. Norville and W. R. Scott, Time-reversal focusing of elastic surface waves, Acoustical Society of America, 118 (2005), 735–744.

[29] K. D. Phung and X. Zhang, Time reversal focusing of the initial state for Kirchhoff plate, SIAM J. Applied Math., 68 (2008), 1535–1556.

[30] C. Prada, E. Kerbrat, D. Cassereau, and M. Fink, Time reversal techniques in ultrasonic nondestructive testing of scattering media, Inverse Problems, 18 (2002), 1761–1773.

[31] A. P. Sarvazyan, O. V. Rudenko, S. C. Swanson, J. B. Fowlkers, and S. V. Emelianovs, Shear wave elasticity imaging: a new ultrasonic technology of medical diagnostics, Ultrasound in Med. & Biol., 24 (1998), 1419-1435.

[32] G. Strang, On the construction and comparison of difference schemes, SIAM J. Numer. Anal., 5 (1968), 506–517.

[33] M. Tanter and M. Fink, Time reversing waves for biomedical Applications, *Mathematical Modeling in Biomedical Imaging I*, Lecture Notes in Mathematics vol. 1983, Springer-Verlag, 2009, pp. 73–97.

[34] J. J. Teng, G. Zhang, and S. X. Huang, Some theoretical problems on variational data assimilation, Appl. Math. Mech., 28 (2007), 581–591.

[35] K. Wapenaar, Retrieving the elastodynamic Green's function of an arbitrary inhomogeneous medium by cross correlation, Phys. Rev. Lett., 93 (2004), 254301.

[36] K. Wapenaar and J. Fokkema, Green's function representations for seismic interferometry, Geophysics, 71 (2006), SI33–SI46.

[37] A. Wiegmann, Fast Poisson, fast Helmholtz and fast linear elastostatic solvers on rectangular parallelepipeds, *Technical Report LBNL-43565*, Lawrence Berkeley National Laboratory, MS 50A-1148, One Cyclotron Rd, Berkeley CA 94720, June 1999.

[38] Y. Xu and L. V. Wang, Time reversal and its application to tomography with diffraction sources, Phys. Rev. Lett., 92 (2004), 033902.